AD-A133 621 ELECTROSTATIC PLUGGING OF MULTIDIPOLE CUSPS(U) AIR 1/1
FORCE INST OF TECH WRIGHT-PATTERSON AFB OH K HENDRICKS
MAY 82 AFIT/CI/NR-82-86T

UNCLASSIFIED F/G 20/9 NL

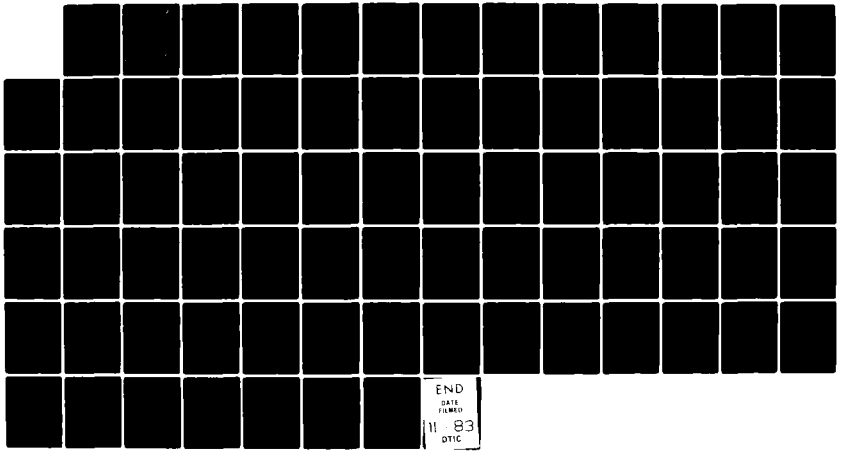

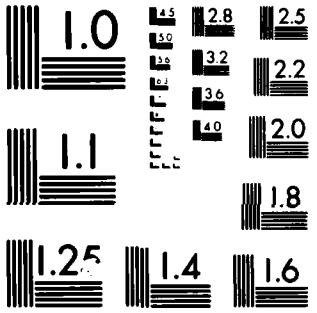

MICROCOPY RESOLUTION TEST CHART
NATIONAL BUREAU OF STANDARDS-1963-A

82-86

AD-A133621

Department of Physics and Astronomy

THE UNIVERSITY OF IOWA

Iowa City, Iowa 52242

83 10 12 184

ELECTROSTATIC PLUGGING OF MULTIDIPOLE CUSPS

by

Kyle Hendricks

A thesis submitted in partial fulfillment
of the requirements for the degree of
Master of Science in Physics
in the Graduate College of
The University of Iowa

May, 1982

Thesis supervisors: Professor Noah Hershkowitz
Associate Professor Raymon T. Carpenter

UNCLASS

SECURITY CLASSIFICATION OF THIS PAGE (When Data Entered)

In AFIT/NR Aug 83

REPORT DOCUMENTATION PAGE		READ INSTRUCTIONS BEFORE COMPLETING FORM
1 REPORT NUMBER AFIT/CI/NR 82-86T	2 GOVT ACCESSION NO AD-A133 621	3 RECIPIENT'S CATALOG NUMBER
4 TITLE (and Subtitle) Electrostatic Plugging of Multidipole Cusps		5 TYPE OF REPORT & PERIOD COVERED THESIS/DISSERTATION
		6 PERFORMING ORG. REPORT NUMBER
7 AUTHOR(s) Kyle Hendricks		8 CONTRACT OR GRANT NUMBER(s)
9 PERFORMING ORGANIZATION NAME AND ADDRESS AFIT STUDENT AT: The University of Iowa		10 PROGRAM ELEMENT PROJECT, TASK AREA & WORK UNIT NUMBERS
11 CONTROLLING OFFICE NAME AND ADDRESS AFIT/NR WPAFB OH 45433		12 REPORT DATE May 1982 13 NUMBER OF PAGES 65
14 MONITORING AGENCY NAME & ADDRESS (if different from Controlling Office)		15 SECURITY CLASS. (of this report) UNCLASS 15a DECLASSIFICATION DOWNGRADING SCHEDULE

16 DISTRIBUTION STATEMENT (of this Report)

APPROVED FOR PUBLIC RELEASE; DISTRIBUTION UNLIMITED

17 DISTRIBUTION STATEMENT (of the abstract entered in Block 20, if different from Report)

Approved for public release IAW AFR 190-17.

Wolaver

Dean for Research and Professional Development
Air Force Institute of Technology (ATO)
Wright-Patterson AFB OH 45433

83

18 SUPPLEMENTARY NOTES

APPROVED FOR PUBLIC RELEASE: IAW AFR 190-17

LYNN E. WOLAVER
Dean for Research and
Professional Development

19 KEY WORDS (Continue on reverse side if necessary and identify by block number)

20 ABSTRACT (Continue on reverse side if necessary and identify by block number)

ATTACHED

DD FORM 1473 EDITION OF NOV 65 IS OBSOLETE

83 10 12 184

UNCLASS

SECURITY CLASSIFICATION OF THIS PAGE (When Data Entered)

Graduate College
The University of Iowa
Iowa City, Iowa

CERTIFICATE OF APPROVAL

MASTER'S THESIS

This is to certify that the Master's thesis of

Kyle Hendricks

has been approved by the Examining Committee for the thesis requirement for the Master of Science degree in Physics at the May, 1982 graduation.

Thesis committee:

Thesis co-supervisor

Thesis co-supervisor

Member

Member

ACKNOWLEDGMENTS

The author wishes to express his appreciation to Professor Noah Hershkowitz and Professor R. T. Carpenter for their guidance, support, and encouragement during this work. I also wish to thank Professor Karl Lonngren, Dr. Peter Coakley, and Dr. Chung Chan for many useful discussions and comments, and many thanks go to Jim DeKock, Steve Cartier, and Randy Goettsch for many helpful discussions and technical assistance. The author is very grateful to Alfred Scheller for construction of the chamber and much of the associated apparatus. Many thanks to Janet R. Kephart for skillfully typing this thesis, and to John Birkbeck and Jeana Wonderlich for their preparation of the figures.

Finally, I wish to thank my family--Carla and Jenna--to whom I dedicate this work.

This work was supported in part by DOE Contract DE-AC02-76ET53034.

ABSTRACT

Electrostatic plugging of multidipole cusps is investigated. The plugging is produced by placing positively biased electrodes on both sides of all magnetic cusps. Experimental observations show the plasma potential follows the electrode potential and the plasma electron density increases by a factor of about two as the electrode bias increases from zero. The addition of a negatively biased grid at one end of the chamber does not change the response of the plasma electron density to the electrode bias. A model, which considers plasma losses along the magnetic cusps as well as by diffusion transverse to the field lines, is shown to qualitatively agree with the data. The elevated interior plasma potential permits the identification and investigation of secondary electron production at the walls. Data is presented which shows that secondary electron emission rate at the chamber walls can be comparable to plasma production rate. A measurement of the relative ion densities of Hydrogen is attempted, but the results are inconclusive as to the effect improved confinement has on the various ion species densities.

TABLE OF CONTENTS

LIST OF FIGURES

I. INTRODUCTION

The use of fields to confine laboratory plasma has been studied for many years. The use of magnetic fields,[1] to increase particle path lengths, is limited by losses along the field lines. For example, the use of cusps and surface magnetic fields has shown that the loss area for ions is bounded by $4r_H L_c$ (Ref. 3) and $2r_i L_c$ (Ref. 4) where $r_H = \sqrt{r_e\, r_i}$, r_i is the ion gyroradius, r_e is the electron gyroradius, and L_c is the length of the magnetic cusps. Attempts using electrostatic fields,[2] to keep either ions or electrons from the chamber walls, have failed because of heating of the grid wires or capacitor plates, used to produce the fields, from plasma bombardment and also because of arcing problems.

To improve plasma confinement, various authors have tried a combination of electrostatic and magnetic confinement. Dolan[5-6] describes this technique as "... magnetic shielding of the grid of an electrostatic plasma confinement device or electrostatic plugging of a magnetic confinement device." Most of this early work has involved ring spindle cusp devices, with electrodes biased negative (with respect to the plasma). The present work is the first attempt at using electrostatic confinement in conjunction with the full line cusp surface magnetic fields.

This work uses a standard 40 liter multi-dipole soup pot in a full line cusp configuration,[1] and uses magnetically shielded electrodes to alter the internal plasma potential structure in a way that improves the plasma confinement.

The apparatus used for this work is described in Section II. This section also describes briefly some of the diagnostic devices used, further descriptions being provided as needed. Section II also discusses the basic operating regime of the device.

Experimental results are presented in Section III. Included are variations of plasma potential, density, and temperature with electrode bias. Also presented are results obtained with the device configured to simulate an ion source.

A simple theory is presented in Section IV which gives good qualitative agreement with the results of Section III.

Section V deals with secondary electron emission from the chamber wall due to electron bombardment. The appearance of the secondary electrons is a result of the way the plasma responds to the biased electrodes when the neutral pressure is less than 10^{-5} Torr.

Section VI is devoted to some experiments using hydrogen as the neutral gas. Hydrogen was used to determine the effect the electrodes had on the ion composition.

Section VII is a final summary of the work presented.

II. APPARATUS

The chamber used for this work was a 40 liter multi-dipole soup pot, with the permanent magnets in a full line cusp arrangement. The magnets produced a maximum field of 1 kilogauss at the poles.

The basic device was modified by placing positively biased (with respect to the chamber wall) electrodes straddling each row of magnets[7] (Fig. 1). The electrodes were approximately 0.7 cm above the wall. At this distance the magnetic field was of order 500 Gauss, so the electrodes were magnetically shielded from the plasma. It was possible to change the gap width from 0.4 cm to 1.3 cm. This separation is on the order of the ion-gyroradius and much greater than the plasma electron gyroradius ($r_i \leq 1$ cm for argon, helium, and hydrogen; $r_e \leq 5 \times 10^{-3}$ cm).

The plasma was produced by electron emission from negatively biased filaments located in the field free interior. The energy of these ionizing electrons (hereafter called primaries) was equal to the difference of the filament bias potential φ_F and the plasma potential φ_p. The device was operated with low electron injection (discharge) currents ($I_d \leq 1$A) which produces densities on the order of 10^{10} cm^{-3}, and low fractional ionization ($\leq 1\%$).

The primary diagnostic tools used were collecting and emitting Langmuir probes. The collecting probes, 1/4" diameter Tantulum discs, were used to measure plasma electron temperature and density, and φ_p in the field free regions. The emissive probe (3 mm long, 0.003 cm diameter, hot tungsten wire) was used to map the spatial plasma potential variation in the device. How we used the probes will be explained more in Section III and Section V.

This work also required the use of mass spectrometers mounted inside and outside the chamber, and a gridded disc for launching pseudo-waves. This apparatus will be discussed more fully in Section VI.

Chamber Operation

The primaries are confined by the surface magnetic field. Previous experiments have shown that the leak width of the primaries is only the order of their gyroradius (0.03 cm for the maximum $|B|$ of 1 kilogauss).[8] Plasma electrons and ions are confined by a combination of magnetic fields and self-consistent electric fields, which for large electrode gaps ($G > r_i$) are essentially the same as those in multidipole devices without electrodes.

Consider operation with the electrodes biased at φ_E such that $e\varphi_E/T_e \gg 1$. For large gaps the plasma potential φ_p will be on the order of T_e/e above ground, which is the anode. As the gap narrows to less than the self-consistent ion leak width the ions will be electrostatically confined at the electrodes and the ion leak width

will be reduced to the gap width or slightly narrower. At the same time the electron leak rate will increase because of the presence of the positively biased electrodes. Improved ion confinement and reduced electron confinement will lead to an increase in the plasma potential until the electron and ion loss rates balance. As the plasma potential increases, electron losses to the wall are greatly reduced (exponentially as $e^{-e\varphi_p/T_e}$) and electron losses to the positive electrodes are increased. Thus the electrodes assume the function of the anode in the plasma and the plasma potential self-consistently adjusts to be within a few T_e/e of the electrode potential.

When $\varphi_p \approx \varphi_E \gg T_e/e$, plasma electrons are electrostatically confined at the cusps, as mentioned above, and plasma electron leaks are then dominated by diffusion across the between cusp magnetic fields to the electrodes. Primaries can still be lost at the cusps and this loss flux has an additional consequence. Cold secondary electrons with energies the order of a few eV are produced by the primaries at the walls and secondary electron currents can be comparable to the current from the primaries.[9] In ordinary multidipole devices these secondary electrons are indistinguishable from the plasma electrons. In this chamber they are distinguishable because the secondaries are accelerated through $e\varphi_p/T_e \gg 1$ before reaching the interior of the device. These essentially monoenergetic electrons are readily confined by the surface magnetic fields, become spatially

isotropic and are readily identified as an additional electron species. See Section V for more details.

The energy of the primaries E_p is equal to $e(\varphi_p - \varphi_F)$ because the plasma serves as a virtual anode for the filaments. Since the plasma potential φ_p generally follows φ_E (and $\varphi_F < 0$), φ_F was varied to keep $\varphi_p - \varphi_F$ = constant. The ionizing electron energy E_p remains essentially constant as φ_E is varied. Although the ionization cross section peaks below 100 eV (e.g., 90 eV for argon);[10] inelastic collisions, multiple ionizations by single electrons, and other factors combine to give a maximum plasma density for E_p greater than 100 eV, and this optimum E_p increase with increasing neutral pressure.[11] Above this energy the density stays close to the maximum value. For this work the primary electron energy E_p was chosen somewhat greater than the value for maximum plasma density so any residual small change in E_p does not have the effect of changing the ionization efficiency.

III. EXPERIMENTAL RESULTS

This section will present the various experimentally determined plasma parameters, plasma potential (φ_p), electron temperature (T_e), and density (n) and their variation with electrode bias (φ_E), neutral pressure (p_o), and electrode separation (G). The operation was confined to two separate modes: 1) multidipole plasma chamber, 2) simulated ion source.

The diagnostics used were emitting and collecting Langmuir probes. The collecting probe was typically placed near the center of the chamber. A voltage was swept across the collecting probe, and an I vs. V Langmuir probe characteristic was generated and recorded on an x - y plotter (Fig. 2). The method of getting parameters from these characteristics involved removing the primary electron portion by drawing the straight line through that part of the trace (Fig. 3). That line is the baseline, the zero current line for plasma electrons (secondary electrons are only observed at pressures lower than those used in this part of the experiment and will be ignored for present), and the natural logarithm of the plasma electron current is plotted against the applied voltage (Fig. 4). This semi-log plot will ideally have two parts. First, a linear part up to φ_p, and a second part that is not collinear with

the first. The voltage where this discontinuity occurs is called the plasma potential. The voltage difference over which I changes by a factor e is the electron temperature T_e.

There is a third parameter measured on the characteristic and that is the plasma saturation current, the value of I at the discontinuity mentioned above. This current can be written[11]

$$I^*_{pe} = e\, n\, A \left(\frac{T_e}{2\pi\, m_e}\right)^{1/2} . \qquad (1)$$

A is the probe area, and T_e is measured in energy units. For a 1/4" diameter probe the density can be written

$$n = 5.8 \times 10^8\, I^*_{pe}/\sqrt{T_e} \qquad (2)$$

where n is in cm^{-3}, I^*_{pe} is in mA, and T_e is in eV. Now we have measured, or calculated the plasma parameters from the characteristic.

Multi-Dipole Operation

First consider the variation of φ_p with applied electrode voltage φ_E (Fig. 5). Note that φ_p generally follows φ_E, although initially $\varphi_p > \varphi_E$; then after $e\varphi_p/T_e \geq 2$ the opposite is true. The difference between the applied voltage and plasma potential is on the order of T_e.

T_e is presented (Fig. 6) as a function of φ_E. T_e is shown to be a fairly constant function of φ_E for a specific parameter set, the error bars on T_e are of the order 1/2 eV. Later it will be assumed (Section IV) that T_e is constant and these data show that this assumption is warranted.

The density also increases as φ_E increases. We call the ratio of the density to its value with zero electrode bias the enhancement ratio (γ). Fig. (7) shows the variation of γ as φ_E increases. Presented also in this figure is the dependence on p_o and gap width. Note the largest ratio of γ is obtained when G = 12 mm and $p_o = 2 \times 10^{-5}$. The lowest value of γ is obtained for $p_o = 1 \times 10^{-4}$ and G = 6 mm. These results for γ can qualitatively be compared to calculated values of γ. This is done in Section IV.

Recall this experiment was initially intended to prove that the electrodes improve the ion confinement, but ions have not been discussed yet. We infer increased ion confinement from the electron density increase. Physically, what is impeding the ion loss? If the ion loss area is reduced then the electrodes are improving the ion confinement.

Looking for the reduction in loss area required making equi-plasma potential contours around the cusp area. Since this area was magnetic, a collecting Langmuir probe couldn't be used. However, Smith et al.[12] showed that an emissive Langmuir probe could give the

desired information. We used the inflection point method they present.

The results are presented in Fig. (8). These results do show the formation of an ion trap. In this case the ion trap reaches 8 volts, but since the ions are very cold a trap of order 1 volt would be sufficient in these devices.

This figure also shows the reduction of the ion loss area. The loss area is defined as $A_L = W_L L_c$ where L_c is the length of the magnetic cusp. W_L is an empirical loss width through which ions with energy $e(\varphi_p)_c + T_i$ can flow out. $(\varphi_p)_c$ means the plasma potential in the center of the device. The upper figure shows this energy is $E_1 = 0.3 + T_i$ and the lower figure shows $E_2 = 42 + T_i$. The corresponding loss widths are $W_{L_1} = 9$ mm and $W_{L_2} = 3$ mm. This analysis was performed for many φ_E, and a linear relationship was found between n and $(W_L)^{-1}$ (Fig. 9).

Simulated Ion Source Operation

Operating the chamber as a simulated ion source was done by covering one end of the cylinder by a grid (or a plate) and removing the magnets and electrodes. We again measured φ_p, n, and T_e as functions of φ_E, p_o. Gap width was set at 12 mm.

Representative data are shown in Fig. (10). The points to notice are: 1) φ_p is slightly less than φ_E at high electrode bias and insensitive to whether the grid is floated or grounded, 2) the

density does saturate, but the saturation occurs at higher φ_E than when the grid is not present, and 3) the factor by which the density increases is greater for the grounded grid case. A simple calculation explaining the variation of density for a grounded and floating grid is presented in the next section.

T_e, for the case shown in Fig. (10), is graphed in Fig. (11). Again, T_e is a fairly constant function of φ_E.

Thus, overall the grid has very little impact on the variation of the measured parameters of the plasma with electrode bias. Of course, the density is reduced because the grid presents a large loss area for ions and electrons, there being no magnetic shielding of the grid. However, the main point is that whether the chamber is operated as an ion-source or multidipole soup pot, the results are qualitatively the same (compare Fig. 7 and Fig. 10).

IV. THEORY

Numerical Estimate

This section will present a simple model that predicts a density increase in qualitative agreement with the experiment. A basic assumption used at this time is that the plasma potential is increased as the electrode bias is increased, and about equal. In the second part of section IV this assumption will be proved.

The quantities to consider are the electron loss rate along the cusp at low electrode bias, and the electron loss rate across the magnetic field at high electrode bias. These quantities are considered because they are the dominant electron loss mechanisms.

The electron loss rate out the cusp can be expressed as:

$$\nu_{eLc} = \frac{n_e v_e}{4} w_c L_c e^{-e\varphi_p/T_e} \tag{3}$$

The ion loss rate can be written:

$$\nu_{ilc} = \frac{j_+}{e} (A_{LC} + A_{fil}) \tag{4}$$

j_+/e is a Bohm loss flux which equals $nc_s/2$. A_{LC} is the ion loss area at the cusps and equals ρL_c. ρ is an effective ion leak which has been shown[3] for similar devices to equal $4\sqrt{r_e r_i}$, L_c is the

total cusp length. A_{fil}, the area of the filaments, is only 0.1% of A_{LC} so we will ignore it. n_e is the total primary and plasma electron density, but the primary density is small so we approximate n_e by n, the interior plasma density. v_e is the electron thermal velocity ($v_e = \sqrt{(T_e/M_e)}$, and c_s is the ion-acoustic velocity ($c_s = \sqrt{T_e/M_i}$). The exponential takes into account electron electrostatic confinement along the cusp. The only quantity undefined is w_c which is an effective electron loss width, and the unknown of the present calculation.

Equating the electron and ion loss rates, because charge neutrality must be maintained, allows expression of w_c in terms of known parameters. Therefore,

$$\frac{n}{4} v_e w_c L_c e^{-e\,4_p/T_e} = \frac{nc_s}{2} 4\sqrt{r_e r_i}\, L_c \tag{5}$$

$$w_c = 8 \frac{c_s}{v_e} \sqrt{r_e r_i}\, e^{e\,\varphi_p/T_e}$$

$$= 8\, r_e \left(\frac{m_e}{m_i} \frac{T_i}{T_e}\right)^{1/4} e^{e\,\varphi_p/T_e} \tag{6}$$

Assuming an argon plasma with $T_e/T_i = 10$ gives

$$w_c = 0.27\, r_e\, e^{e\,\varphi_p/T_e} \tag{7}$$

Of course, w_c is determined by physics other than that involving the interior plasma potential φ_p. In fact, if w_c is determined, then this equation determines the plasma potential such that the electron and ion loss rates are balanced. For example, using $w_c = r_e$, then gives $e\,\varphi_p = 1.29\,T_e$, a result which is very close to that experimentally observed in the present work. Thus, w_c cannot be greatly different from r_e or the predicted plasma potential will not agree with the data. Furthermore, in a discussion of the properties of the systems as the electrode bias is changed, the electron loss along the cusp will be completely dominated by the exponential terms in Eq. (1) so the exact value used for w_c is unimportant. Therefore, we take $w_c = r_e$ in the following and write

$$\nu_{eLc} = \frac{n}{4} v_e\, r_e\, L_c\, e^{-e\varphi_p/T_e} \quad . \tag{8}$$

Now consider the case $e\,\varphi_p/T_e \gg 1$. This, of course, results from a high electrode bias. In this regime the electrons are electrostatically trapped along the cusp, so the only loss process for electrons is diffusion across the magnetic field lines.

Dolan defines a characteristic time for electron loss by spatial diffusion to be:[13]

$$\tau_d = \frac{\text{(total number of electrons)}}{\text{(number lost per second by diffusion)}}$$

$$= \frac{\int d\vec{x}\, n}{\int d\vec{a} \cdot (-D \nabla n)} \tag{9}$$

where $d\vec{x}$ is a volume element and $d\vec{a}$ is a surface element of the plasma. The surface element can be written da = Ldl where L is the height of the plasma cylinder and dl is along the magnetic field. Now

$$\int d\vec{x}\, n = n L \pi r_p^2 \tag{10}$$

with r_p the radius of a cross section of plasma.

The diffusion coefficient is given by:[14]

$$D = \frac{m_e T_e}{e^2 B^2} \nu_c \tag{11}$$

where ν_c is the effective momentum-transfer collision frequency for electrons with ions, neutrals, and $\vec{E}$ field fluctuations in the limit $\nu_c \ll \omega_{ce}$. The density gradient may be approximated:

$$-\nabla n \approx n/\xi_1 \tag{12}$$

where ξ_1 is the distance between flux surfaces ψ_0 and ψ_1 (Fig. 12). ψ_1 is the flux surface that just touches the inner edge of the

electrode, and ψ_0 is a flux surface that is a distance r_e from the center of the magnetic cusp.

Plugging these factors into Eq. (9) gives

$$\tau_d = \frac{\pi r_p^2 e^2/m_e}{\int d\ell\, T_e \nu_c/\xi_1 B^2} \quad . \tag{13}$$

Let ξ_0 and B_0 be the values of ξ_1 and B at any arbitrary reference point (Fig. 12). By magnetic flux conservation:

$$\xi_1 B = \xi_0 B_0 \quad . \tag{14}$$

ν_c and T_e are constant in the main plasma volume because the central plasma is field-free and uniform. We will assume that ν_c and T_e are constant all along ψ_1. By definition $dl' = d\ell/2\pi r_p$ and $B' = B/B_0$. Then:

$$\tau_d = \frac{e^2 B_o^2 \xi_0 r_p}{2m_e T_e \nu_c X} = \frac{\xi_0 r_p}{\rho_o^2 \nu_c X} \quad . \tag{15}$$

X is written:[13]

$$X = N \int_{\psi_1} \frac{d\ell'}{B'} \approx 1 \tag{16}$$

N is the number of magnetic cusps, and ρ_o is the electron gyro-radius at the reference point where ξ_0 and B_o are evaluated.

The cross field leak rate for electrons is defined

$$\nu_{eLT} = \frac{nV}{\tau_d} \tag{17}$$

where V is the plasma volume. Now substituting τ_d gives:

$$\nu_{eLT} = nV \frac{\rho_o^2 \nu_c}{\xi_0 r_p} e^{- g\, e(\varphi_p - \varphi_E)/T_e} \quad . \tag{18}$$

Now V/r_p = A the surface area of the plasma:

$$A = SL_c \quad , \tag{19}$$

with S the distance between cusps ($\approx$ 8 cm) and L_c the magnetic cusp length. Now ξ_0 is the order of half the electrode gap G. The electron gyro-radius at the boundary ψ_1 can be written $\rho_0 = v_e/\Omega$ where Ω is electron cyclotron frequency. The exponential is again an electrostatic confinement factor with

$$g = \begin{cases} 1 & \varphi_p > \varphi_E \\ 0 & \varphi_E > \varphi_p \end{cases}$$

N is the number of magnetic cusps, and ρ_o is the electron gyro-radius at the reference point where ξ_0 and B_o are evaluated.

The cross field leak rate for electrons is defined

$$\nu_{eLT} = \frac{nV}{\tau_d} \tag{17}$$

where V is the plasma volume. Now substituting τ_d gives:

$$\nu_{eLT} = nV \frac{\rho_o^2 \nu_c}{\xi_0 r_p} e^{-g\, e(\varphi_p - \varphi_E)/T_e} \quad . \tag{18}$$

Now $V/r_p = A$ the surface area of the plasma:

$$A = SL_c \quad , \tag{19}$$

with S the distance between cusps (≈ 8 cm) and L_c the magnetic cusp length. Now ξ_0 is the order of half the electrode gap G. The electron gyro-radius at the boundary ψ_1 can be written $\rho_0 = v_e/\Omega$ where Ω is electron cyclotron frequency. The exponential is again an electrostatic confinement factor with

$$g = \begin{cases} 1 & \varphi_p > \varphi_E \\ 0 & \varphi_E > \varphi_p \end{cases}$$

The cross field leak rate is:

$$\nu_{eLT} = n\, v_e\, r_e\, L_c \cdot \left(\frac{\nu_e}{\Omega} \cdot \frac{\mathfrak{S}}{G}\right) e^{-g\, e(\varphi_p - \varphi_E)/T_e} \quad , \tag{20}$$

$$\equiv \frac{n}{4}\, v_e\, w_T\, L_c\, e^{-g\, e(\varphi_p - \varphi_E)/T_e} \quad . \tag{21}$$

Where in the last equation we define an effective cross-field leak width, w_T, given by

$$w_T = 4 r_e \frac{\nu_c}{\Omega} \frac{\mathfrak{S}}{G} \quad . \tag{22}$$

ν_c can be written, ignoring E field fluctuations, as

$$\nu_e = \nu_{ei} + \nu_{en} \tag{23}$$

where ν_{ei} is the electron-ion collision frequency and ν_{en} is the electron-neutral collision frequency. ν_{ei} and ν_{en} are estimated as:[15]

$$\nu_{ei} = 4 \times 10^{-5}\, n/T_e^{3/2} \tag{24}$$

$$\nu_{en} = 5.5 \times 10^{8}\, p_o\, T_e^{3/2} \tag{25}$$

The density n is measured in cm^{-3}, p_o in Torr, T_e in eV, and ν in sec^{-1}.

Ω is the cyclotron frequency evaluated midway between the cusps. Measuring the field strength along ψ_1 it was found that $|\vec{B}|$ at this point is approximately 20 Gauss. Taking $|\vec{B}| = 0$ in the interior, we see an average $|\vec{B}|$ for electron diffusion is 10 Gauss. This gives $\Omega = 1.8 \times 10^8$ rad/sec.

Now taking the ratio of w_c and w_T, assuming $T_e \sim 3$ eV gives

$$\frac{w_c}{w_T} = \frac{r_e}{4r_e \frac{\nu_c}{\Omega} \frac{2S}{G}} = \frac{G\Omega}{8S\nu_c} = (2.8 \times 10^6 \text{ G})$$

$$\times (7.7 \times 10^{-6} n + 2.86 \times 10^9 p_o)^{-1} \quad . \qquad (26)$$

This expression with w_c/w_T normalized to G is graphed in Fig. (13). This graph shows that for $p_o \sim 10^{-4}$ and 10^9 $cm^{-3} \leq n \leq 10^{10}$ cm^{-3} then $(w_c/w_T)/G \sim 8$. Since 0.6 cm $\leq G \leq$ 1.2 cm we see that $4.8 \leq w_c/w_T \leq 9.6$.

In general, plasma density is determined by a balance of plasma production and losses. The creation rate of plasma electrons can be written as βI_d where I_d is the filament discharge current and β depends on the cross section for ionizing and nonionizing collisions, and on the primary electron confinement time. During an individual experiment βI_d was constant, independent of φ_E, therefore

$$\beta I_d = \nu_{eLc} + \nu_{eLT} \quad . \tag{27}$$

When $\varphi_E = 0$ and $e\,\varphi_p/T_e \sim 1$ means $\beta I_d \sim \nu_{eLc}$, but when $\varphi_E \sim \varphi_p \gg T_e/e$ ($\varphi_E \sim \varphi_p$ will be proved later) then $\beta I_d \sim \nu_{eLT}$. The last sentence refers only to the dominant loss mechanism at a given limit for φ_E. Equating the two loss rates shows

$$\frac{n(0)}{4} v_e w_c L_c e^{-e\,\varphi_p(0)/T_e} = \frac{n_H}{4} v_e w_T L_c \quad . \tag{28}$$

The density ratio is

$$\frac{n_H}{n(0)} = \frac{w_c}{w_T} e^{-e\,\varphi_p(0)/T_e} \sim 0.27 \frac{w_c}{w_T} \quad . \tag{29}$$

Using the limits of w_c/w_T means

$$1.25 \leq \frac{n_H}{n_o} \leq 2.5 \quad . \tag{30}$$

These values are in excellent agreement with the ratios observed in Fig. (7).

At sufficiently high neutral pressure or low plasma density where electron-neutral collisions dominate $(\nu_{eLc}/\nu_{eLT}) \alpha\, G/\nu_{en} \alpha\, G/p_o$. However, if we consider the case of $\nu_{ei} \gg \nu_{en}$ then

$$\frac{\nu_{eLc}}{\nu_{eLT}} \alpha \frac{G}{\nu_{ei}} \alpha \frac{G}{n} \quad . \tag{31}$$

Here the effective cross field leak rate ν_{eLT} is proportional to the plasma density so the steady state density ratio is no longer proportional to the ratio given by Eq. (29). The neutral pressure and density at which the transition from $\nu_{en} >> \nu_{ei}$ to $\nu_{ei} >> \nu_{en}$ depends on the particular plasma species and electron temperature. The dependence of the enhancement ratio on the gap width G and the discharge current I_d can be seen as follows. At high electrode bias the balance of electron production and loss (when $\nu_{ei} >> \nu_{en}$) can be expressed:

$$\beta I_d \alpha n_H v_e r_e L_c \frac{n_H}{G} \tag{32}$$

so the density at high electrode bias goes like $n_H \alpha \sqrt{I_d G}$. At low electrode bias, when losses along the cusp dominate, the density is proportional to I_d so the ratio of density at high electrode bias to zero bias is:

$$\frac{n_H}{n_o} \alpha \frac{\sqrt{I_d G}}{I_d} = \sqrt{\frac{G}{I_d}} \quad , \tag{33}$$

in agreement with Fig. (7).

Variation of n with φ_E in a Multi-Dipole Field

The dependence of the density on electrode bias can be determined from:

$$\beta I_d = \frac{n}{4} v_e L_c [w_c e^{- e \varphi_p / T_e} + w_T e^{- 2e(\varphi_p - \varphi_E)/T_e}] \quad . \quad (34a)$$

However, Eq. (34a) requires a relationship between φ_p and φ_E. To find this relationship requires equating electron production and loss

$$\frac{n}{4} v_e L_c [w_c e^{- e \varphi_p / T_e} + w_T e^{- g\, e(\varphi_p - \varphi_E)/T_e}]$$

$$= \frac{n}{2} c_s \sqrt{4 r_e r_i}\, L_c R(\varphi_p, \varphi_E) \quad . \quad (34b)$$

where R is a retardation factor that is unknown, and $\nu_{en} \gg \nu_{ei}$ is assumed. This equation can be reduced to

$$e^{- e \varphi_p / T_e} + \frac{1}{8} e^{- g\, e(\varphi_p - \varphi_E)/T_e} = 0.27\, R \quad (35)$$

where $w_c / w_T \sim 8$ has been used.

Consider first $\varphi_E = 0$, but $\varphi_p > 0$ then Eq. (35) can be written

$$\frac{9}{8} e^{- e \varphi_p / T_e} = 0.27 \quad (36)$$

where R = 1 because the ions are lost by an unimpeded Bohm flux. Therefore

$$e\,\varphi_p/T_e = 1.4 \equiv e\,\varphi_p(0)/T_e \quad .$$

Consider now $\varphi_E > 0$, but $\varphi_p = \varphi_p(0)$. When $\varphi_E = \varphi_p(0)$ Eq. (37) becomes

$$\frac{8}{9}(0.27) + \frac{1}{8} = 0.27\ R = 0.3678 \quad , \tag{38}$$

or implies R > 1. However, R ≤ 1 so φ_p must increase as some function of φ_E to keep R ≤ 1. Since this function is unknown R cannot be calculated, but limits of R can be obtained.

Assume initially that R = 1 and $\varphi_p > \varphi_E$. Therefore Eq. (39) is, solving for φ_p:

$$e\,\varphi_p/T_e = \ln\left(\frac{1 + \frac{1}{8}\,e^{\,e\,\varphi_E/T_e}}{0.27}\right) \quad . \tag{40}$$

This equation satisfies $\varphi_p > \varphi_E$ only if $e\,\varphi_E/T_e \leq 2$. Therefore, R must be less than 1 when $e\,\varphi_E/T_e > 2$. Let us now look for R, such that $\varphi_E = \varphi_p$ and define this $R = R_{max}$. Therefore, Eq. (35) becomes

$$e^{-\,e\,\varphi_E/T_e} + \frac{1}{8} = 0.27\ R_{max} \tag{41}$$

or $R_{max} = 3.7(1/8 + e^{-e\varphi_E/T_e})$. For this experiment $0 \leq e\varphi_E/T_e \leq 20$ ($T_e \sim 3$ eV), therefore, $0.46 \leq R_{max} \leq 1.0$.

Consider $\varphi_p < \varphi_E$, now the only relationship between φ_p and φ_E is through R. This regime is the case considered in Eq. (40) with φ_p replacing φ_E. That is, for R as large as is physically possible, $\varphi_p = \varphi_E$. We conclude that even if ion losses are retarded only to the extent that they can physically balance electron losses, we must have $\varphi_E \sim \varphi_p$.

The <u>smallest</u> R that is physically reasonable occurs when the cusps are plugged by the electrode potential then

$$R = e^{-he(\varphi_E - \varphi_p)/T_i} \tag{42}$$

where

$$h = \begin{cases} 1 & \varphi_E > \varphi_p \\ 0 & \varphi_E < \varphi_p \end{cases} .$$

Eq. (35) can be written

$$e^{-e\varphi_p/T_e} + \frac{1}{8} e^{-ge(\varphi_p - \varphi_E)/T_e} = 0.27\, e^{-he(\varphi_E - \varphi_p)/T_i} . \tag{43}$$

Note if $g = 1$ then $h = 0$ and vice versa. There cannot be plugging for electrons and ions at the same time. Eq. (43) can be solved

numerically for φ_p as a function of φ_E. The solution set of Eq. (43), for $T_e/T_i = 10$ and $\varphi_p < \varphi_E$, is that $e(\varphi_E - \varphi_p) < T_e$ and $e(\varphi_E - \varphi_p)$ is largest when $e\,\varphi_E/T_e \sim 20$ [i.e., $e(\varphi_E - \varphi_p) = 0.08\ T_e$]. So the plasma potential is slightly less than the electrode potential. We conclude from this that at elevated values of φ_E, $\varphi_p \sim \varphi_E$ and we will assume equality in the following.

Let us now consider the density dependence on φ_E. Using $w_T/w_c = 1/8$, and $\varphi_E = \varphi_p \gg 0$, the balance of electron production and loss gives

$$\beta I_d = \frac{n}{4} v_e L_c w_c [e^{-e\,\varphi_E/T_e} + \frac{1}{8}] \quad . \tag{44}$$

When $\varphi_E = 0$ then

$$\beta I_d \approx \frac{n(0)}{4} v_e L_c w_c (1 + \frac{1}{8})\, e^{-e\,\varphi_p(0)/T_e} \quad . \tag{45}$$

The density ratio is

$$\frac{n}{n(0)} = \frac{9}{8} \frac{e^{-e\,\varphi_p(0)/T_e}}{e^{-e\,\varphi_E/T_e} + 1/8} \quad . \tag{46}$$

This equation is graphed in Fig. (13).

Now assume $\nu_{ei} \gg \nu_{en}$ then Eq. (44) becomes

$$\beta I_d \approx \frac{n}{4} v_e L_c w_c (e^{-e\,\varphi_E/T_e} + \frac{n}{8n(0)}) \tag{47}$$

where $\varphi_E \approx \varphi_p >> 0$. Then:

$$\frac{n}{n(0)} = \frac{9}{8} \frac{e^{-e\,\varphi_p(0)/T_e}}{e^{-e\,\varphi_E/T_e} + \frac{n}{8n(0)}} \tag{48}$$

This expression is also graphed in Fig. (13).

The above considerations show that a theory assuming the main loss mechanism for electrons at large φ_E is cross field diffusion gives very good qualitative agreement with the experimental results of Section III.

Variation of n with φ_E in the Presence of an Extraction Grid

Now consider a problem similar to the one just discussed, but where one end of e-pot is replaced by a grid or metal plate. The calculations discussed here will show good qualitative agreement with experimental results presented earlier about simulated ion-source operation.

First, consider the potential of a floating grid. The ion current to such a grid with area A_g and at a potential φ_g can be estimated to be $I_g = e\,n\,c_s\,A_g/2$ provided $\varphi_p > \varphi_g$. I_g will only have variation with n, as we showed earlier T_e is constant, and A_g is constant. When the grid potential $\varphi_g = \varphi_f$ the plasma floating potential, the plasma must supply electron current to balance the ion current. At high neutral pressure where the density of the primary electrons is much less than the plasma density this balance gives

$$n A_g \sqrt{\frac{T_e}{2\pi m_e}} e^{-e(\varphi_p - \varphi_f)/T_e} = \frac{n}{2} A_g \sqrt{\frac{T_e}{m_i}} \tag{49}$$

or solving for $\varphi_p - \varphi_f$ gives

$$\varphi_p - \varphi_f = \frac{T_e}{e} \ln 2\sqrt{\frac{m_i}{m_e 2\pi}} \approx 5\ T_e/e \tag{50}$$

for an argon plasma. However, at low neutral pressure the primary electrons, with energy E_p, contribute a current I_p given by:[8]

$$I_p = e\ n_p\ A_g\ \overline{v \cos\theta} \tag{51}$$

where

$$\overline{v \cos\theta} = \int d\vec{v}\ f(\vec{v}) v \cos\theta \tag{52}$$

The distribution function $f(\vec{v})$ is characterized as a shell in velocity space[16-17]

$$f(\vec{v}) = \frac{\delta(v - v_p)}{4\pi v_p^2} \tag{53}$$

where v_p is primary electron velocity. Therefore

$$\overline{v \cos \theta} = \frac{1}{2} v_p \left(\frac{1}{2} - \frac{eV}{m v_p^2}\right) \tag{54}$$

where $eV = e(\varphi_p - \varphi_g)$. Then the expression for I_p is

$$I_p = e n_p \frac{v_p}{4} A_g \left(\frac{E_p - e(\varphi_p - \varphi_g)}{E_p}\right) \tag{55}$$

$$= \frac{e n_p}{4} A_g \sqrt{\frac{2 E_p}{m_e}} \left(\frac{E_p - e(\varphi_p - \varphi_g)}{E_p}\right) \tag{56}$$

The current balance gives

$$\frac{e n_p}{4} A_g \sqrt{\frac{2 E_p}{m_e}} \left(\frac{E_p - e(\varphi_p - \varphi_g)}{E_p}\right) + e n A_g \sqrt{\frac{T_e}{2\pi m_c}} e^{-e(\varphi_p - \varphi_g)/T_e}$$

$$= \frac{en}{2} \sqrt{\frac{T_e}{m_i}} A_g \tag{57}$$

Since the right hand side of Eq. (49) is the same as Eq. (57) requires that $\varphi_p - \varphi_g$ must increase (reducing the plasma electron current). This trend in $\varphi_p - \varphi_g$ is shown in Fig. (14).

A similar calculation as was used earlier this section can employed to calculate the density variation with φ_E when the grid is in place. With a floating grid the balance of electron production and loss can be written

$$\beta I_d = n_f \frac{v_e L_c}{4} [w_c e^{- e \varphi_p / T_e} + w_T] + n_f c_s \frac{A_g}{2} \qquad (58)$$

or

$$n_f \alpha [w_c e^{- e\varphi_p / T_e} + w_T + 2 c_s A_g / v_e L_c]^{-1} \qquad (59)$$

This expression ignores primary electrons so is only valid at high pressure. This equation also shows that density is reduced by the presence of the grid, but the variation with φ_E is not qualitatively changed.

If the grid is grounded, in the same limit as the floating grid case, the density varies as:

$$n_{gn} \alpha (w_c e^{- e \varphi_p / T_e} + w_T + \frac{4 A_g}{L_c} e^{- e \varphi_p / T_e})^{-1} \quad . \qquad (60)$$

When $\varphi_g < 0$ electron current will be less than when $\varphi_g = 0$. Then the last term in the expression for n_f will be less than for the last term in Eq. (60). Then the ratio of $(n_f/n_{gn}) < 1$. If $\varphi_g > 0$ the opposite holds and $n_f/n_{gn} > 1$. These arguments are in qualitative agreement with the data shown earlier in Fig. (10).

V. SECONDARY ELECTRONS

One consequence of the elevated interior plasma potential is the observation of secondary electrons by primary electron bombardment of the chamber walls. These secondary electrons have a characteristic signature in the Langmuir probe trace that is clearly distinct from the plasma and primary electron contributions.

The physical picture is a cold electron produced at the wall being accelerated through the plasma-wall sheath at the gap and forming a shell in velocity space at $v = \sqrt{2\ e\ \varphi_p/M_e}$. In ordinary multi-dipole devices this velocity is of order $\sqrt{Te/M_e}$ and the secondaries merely spread out the Maxwellian plasma. The signature left by secondary electrons, when projected onto a planar probe, is a straight line starting at $\varphi = 0$ (Fig. 15). This straight line is most easily seen when $P_o < 1 \times 10^{-5}$. At the lower pressure, the density of primaries, and therefore secondaries, is a large fraction of the total electron density and therefore easily observed. Also, at these low pressures the secondaries do not readily thermalize with the plasma electrons.

The number of secondaries produced per incident primary is called the yield (δ). The δ wanted is for production at the wall and should not include production at the probe.

The probe current can be written

$$I \propto \int_{v_{min}}^{\infty} vf(v)[1 - \delta(v_w)]dv \tag{61}$$

where $\delta(v_w)$ is the ratio of secondary current to primary current. The velocity of electrons at the probe, v_w, goes to zero when $v = v_{min}$. Energy conservation gives $v^2 + 2\,e\,\varphi_{pr}/m = v_w^2$ so $v_{min} = \sqrt{-2\,e\,\varphi_{pr}/m}$ where φ_{pr} is the probe bias and e/m is electron charge to mass ratio. f(v) is the velocity distribution for a shell of monoenergetic electrons projected onto a one dimensional probe[18] or

$$f(v) \propto \begin{cases} 1 & 0 \leq v \leq v_p \\ 0 & v_p < v \end{cases} \tag{62}$$

where v_p is the primary electron velocity. $\delta(v_w)$ is known to vary with bombarding energy as shown in Fig. 16. For simplicity we assume

$$\delta(v_w) \approx \left(\frac{v_w}{v_u}\right)^2 \tag{63}$$

where v_u is defined by $E_u = 1/2\ Mv_u^2$, and E_u is the secondary electron energy such that $\delta = 1$ (Fig. 16). Thus, the probe current is

$$I \propto \int_{v_{min}}^{v_p} v\left(1 - \frac{v^2 + 2\,e\,\varphi_{pr}/m}{v_u^2}\right) dv \tag{64}$$

or

$$I \propto \frac{1}{mE_u}\{(E_p + e\,\varphi_{pr})(E_u - e\,\varphi_{pr}) - \tfrac{1}{2}(E_p^2 - e^2\,\varphi_{pr}^2)\} \quad (65)$$

where $E_p = (1/2)\,mv_p^2$. The primary electron current to the probe when the probe is biased at φ_p, is the saturation current $I_p^* \propto (E_p + e\,\varphi_p)/m$.

Hachenberg and Brauer[19] list $E_u \approx 200$ V for tantalum, which the probe was made from. The assumed form for $\delta(v_w)$ is a slight underestimation, but the maximum error is about 25% at $E_p = 70$ eV. A representative probe trace which exhibits all three electron species and effects from the probe is shown in Fig. (16). Note the saturation currents of the three components are comparable and that the reduction in the apparent primary electron current is significant. The fit of the three components is not sensitive to the yield coefficient used for secondary electrons emitted at the probe.

Now that the saturation currents have been corrected they can be used to calculate the yield coefficient at the chamber walls. Secondaries are created at a rate given by $\delta n_p v_p A_p$ where n_p is the density of primaries, v_p is primary electron velocity, and A_p is primary loss area. Secondaries are lost either to the walls (A_s) or by inelastic processes identical to those involving primaries. If the secondaries cause an ionization they lose enough energy to be trapped and then lost by diffusion (recall Section IV). Balancing production and loss gives

$$\delta n_p v_p A_p = n_s v_s (A_s + V\sigma_i n_o) \tag{66}$$

where V is the plasma volume, n_o is the neutral density and σ_i is the ionization cross section. The probe saturation currents for primaries and secondaries, I^*, are proportional to nv so Eq. (66) gives

$$\delta = \frac{I_s^*}{I_p^*} \left[\frac{A_s + V \sigma_i n_o}{A_p}\right] \tag{67}$$

The term $A_p = r_p L_c$ where r_p is the primary electron gyroradius, and L_c is total length of the magnetic cusps. Now $r_p = 2.4\sqrt{2E_p/B}$. Recall from Section II that at the wall B ~ 1 kilogauss so $r_p = 3.4 \times 10^{-3} \sqrt{E_p}$. A typical energy for primaries is $E_p \sim 100$ eV or $A_p = 27$ cm^2.

The numerator of the bracketed term is not as easily calculated. It is possible for A_s to be as small as $r_s L_c$ or as large as GL_c where r_s is the secondary electron gyroradius and G is the electrode gap, so 6 cm^2 $\leq A_s \leq$ 800 cm^2. The ionization term, for an argon plasma at neutral pressure p_o, can be evaluated using $V = 2.2 \times 10^4$ cm^3, $\sigma_i = 2.4 \times 10^{-16}$ cm^2, and $n_o = 3 \times 10^{16}\ p_o$ (Torr) or

$$V\sigma_i n_o \approx 1.6 \times 10^5\ p_o(\text{Torr}) \tag{68}$$

At $p_o = 5 \times 10^{-6}$ Torr, this term is .8 cm^2. Therefore the ionization is negligible if $A_s = 800$ cm^2 and non-negligible if $A_s = 8$ cm^2. The extreme estimates of the bracketed term gives 0.33 and 30.0. Although E_p varied for data in this experiment, E_s is determined by the details of secondary emission and essentially constant so the bracketed term can be written $\alpha/\sqrt{E_p}$.

Experimental values of I_s^*/I_p^* are shown in Fig. (17). The values of I_s^*/I_p^* are comparable to 1.0 so the minimum value of δ for $E_p = 100$ eV is 0.33. A graph (Fig. 17) of $\delta = (I_s^*/I_p^*)\ 10/\sqrt{E_p}$ shows the general initial trend for δ, where 10 is a representative value taken for the numerator of the bracketed term in Eq. (67).

The above argument has shown that primaries can produce a significant number of secondaries. However, the main point was to consider the secondary electron contribution to the plasma. The production rate of secondaries is $\delta n_p v_p A_p$ while the production of plasma electrons is $n_p v_p \sigma_i n_o V$, ignoring primary and secondary electrons degraded in energy by collisions. The ratio of secondary production to plasma production is $\delta A_p/V \sigma_i n_o = 34\delta$ when $A_p = 27$ cm^2 and $p_o = 5 \times 10^{-6}$ Torr. Using the minimum of 0.33 for δ means that $\delta A_p/V\sigma_i n_o \geq 10$ so more electrons are being produced by secondary emission than by ionization.

It has been shown that plasma electrons are electrostatically confined at the cusps and losses occur by diffusion between the cusps. The secondaries are not electrostatically confined unless they lose energy. The ratio of density of secondary electrons to

plasma electrons can be quite high and their probe saturation currents can be comparable. Since in conventional multidipole devices $e\,\varphi_p/T_e \approx 1$, the confinement of plasma and secondary electrons is essentially the same and this means neglecting the secondary electrons could introduce large errors in calculations involving plasma production and loss rates.

Secondary electrons have not been considered in previous multidipole experiments because they are indistinguishable from plasma electrons when wall sheaths are small. In addition, at high neutral pressures primary electron densities are relatively low. The presence of secondary electrons is not negligible for low neutral pressure regimes. Calculations of particle and energy balance in multidipole devices that do not take secondaries into account can result in significant errors. Secondary electrons are also important in interpreting Langmuir probe data. It is apparent that the secondary electrons emitted from the probe can lead to substantial misjudgement of the primary electron saturation current and consequently the plasma electron temperature (Fig. 4).

VI. RELATIVE ION DENSITIES

This section deals with experiments where the relative density of the various ions species are observed. Directly measuring the relative ion densities would give clear evidence concerning effectiveness of electrodes in confining the ions. Showing that the atomic ion density increases with electrode bias relative to the molecular ion density could have a large effect on whether ion sources[20] for neutral beam injectors are modified with electrostatic plugging. Unfortunately, this measurement could not be performed. The relative density measurement was attempted by three methods: 1) mass spectrometer mounted outside the chamber, 2) particle bursts called pseudo-waves, and 3) mass spectrometer mounted inside the plasma volume.

Theory

The idea behind a mass spectrometer is fairly well known, but to refresh the reader's memory the ideas are repeated. Consider a particle with mass number A and atomic number Z with energy $Ze\varphi$. The velocity of this particle is then $v = \sqrt{2\ Ze\varphi/Am_p}$ where m_p is the proton mass. The magnetic field B required to turn the particle in a circle of radius r as given by the Lorentz force is $A\ m_p\ v^2/r = (Ze/c) \times vB$. There is then a linear relationship between B^2 and $e\varphi$. The slope is given by $(2\ m_p c^2/e^2\ r^2) \times (A/Z)$. In the mass spectrometers

used here, r was kept constant and ions, assumed monoenergetic, were detected after being bent through 180° as B was varied. Flux peaks were observed at certain values of B for given φ and A. By plotting these critical B values against φ_p, the slope of the lines were determined. Then the ratio of the slopes is equal to the ratios of $(A/Z)_i/(A/Z)_j$ where i and j refer to specific ion species. The slopes allow identification of the ion species, but no information about the density. The density comes from the area under the peak observed with the spectrograph. This area was approximated by using the full width at half maximum (FWHM) multiplied by the maximum amplitude of the peak.

The other method involved the use of particle bursts called pseudo-waves. Pseudo-waves were first seen by Alexeff et al.[21] in 1968. These waves were launched as a result of negative potential pulses applied to a grid. They explained the launching of pseudo-waves from a grid by considering an ion falling through a negative potential well, produced by the grid wire. If the pulse was removed while the ion was at the bottom of the negative well, then the ion will travel on with a velocity $v_{max} = (2\, e\varphi_{max}/Am_p)^{\frac{1}{2}}$ where φ_{max} is the maximum amplitude of the pulse and a singly charged ion is assumed. Likewise, if the particle is somewhere else in the well the velocity is $v = \sqrt{2\, e\varphi/Am_p}$ where φ is the local pulse amplitude. Also, positive pulses will work as a pusher of ions away from the grid.

The reason ion species identification is possible is that heavier ions will travel slower so that the ion species will become

separate far from the launcher. This characteristic is inherent in all waves, however, only pseudo-waves will show a change of velocity with pulse amplitude. If you look at the current collected by the receiver the time interval between the direct coupled signal and the pseudo-wave will decrease as φ_{max} is increased and vice versa. So the identification of pseudo-waves is possible and the identification of a pseudo-wave for a particular species is possible. The density is calculated the same as for the mass spectrometer.

Experimental Results

External Mass Spec.

The external spectrometer was approximately nine inches from the plasma anode, and the beam line connecting the spectrometer to the chamber was sheathed in μ-metal to eliminate the fringing field in the tube. The gyroradius was 4 cm, and the maximum magnetic field strength was in excess of 2 kilogauss. The electromagnet was powered by a programmable power supply, which was swept by a sawtooth from an oscilloscope (Fig. 18).

The spectrographs were recorded on an x-y plotter where the x axis was the output of the programmable power supply, and the y axis was the output of an electrometer which showed the ion current collected.

A typical spectrograph is shown in Fig. (19) and the magnetic field for each ion species is marked on the respective x axis. These

values for B are used in the B^2 versus φ plots to identify the ion species (Fig. 20).

Knowing A/Z, and assuming Z = 1 for a hydrogen plasma, allowed identification of H_1^+, H_2^+, and H_3^+. The quantity of interest is the ratio of fluxes for H_1^+ and H_2^+. The ratio (R) is found by measuring the areas under the H_1^+ and H_2^+ peaks (Fig. 19). From several spectrographs it is possible to see the variation of R with φ_E (Fig. 20).

Depending on the choice of p_o and φ_f the graph of R versus φ_E could be made to do anything. However, taking $\varphi_p - \varphi_f = 90$ V and $p_o = 4 \times 10^{-5}$ Torr, the curve of the ratio follows very well with the curve for plasma electron density (Fig. 7).

There are several difficulties in using an external spectrometer. The beam line from the chamber to the spectrometer places the exit port in the middle of a magnetic cusp line. The influence of the surface magnetic field could greatly alter the ion extraction at low ion velocities and would be different for different masses. Also, the long path length allows the possibility of charge exchange collisions and a change in the ion spectra.

Because of these possible errors a method for determining the ion species composition needed to be carried out inside the chamber.

Pseudo-Waves

The pseudo-waves were launched from a grid with a diameter of 1.8 cm with 60 lines/inch. The collected current was displayed

on an oscilloscope using a high gain plug-in. The pseudo-waves were located by varying the pulse amplitude and locating a wave that moved properly. Once the waves were found, photographs were taken of the display screen for measurements.

During the analysis only one pseudo-wave was observed. This pseudo-wave had a velocity that an H_2^+ ion would have if launched from the tail of the pulse sheath. A pseudo-wave for a H_1^+ ion was not observed because the velocity of such an ion would be buried in the directly coupled signal of the pulse, or if the distance traveled by the wave was such that the wave was not buried then damping would kill the wave before it could be detected. Due to the pseudo-wave not being observed an internal mass spectrometer was built.

Internal Spectrometer

The internal spectrometer constructed was based on the design of Ehlers et al.[22] This spectrometer could produce a magnetic field in excess of 1 kilo-gauss with a fringing field below 100 Gauss. The field was produced by two coils with each coil made of 550 turns of 28 gauge enamel insulated wire. Between the pole faces a copper box was used to short out electric fields where the ion current was measured. The internal spectrometer had a 1.5 cm gyroradius and a two grid entrance aperture. The outer grid was used to keep out primary and plasma electrons, the inner grid was used to retard the ion energy. The ion energy had to be reduced so the magnetic field, lowered by heating, could bend the ion orbit in the required semi-circle.

This measurement was also inconclusive due to the poor resolution of the spectrometer. The poor resolution was a result of the fringing field, and that the particle orbit was poorly defined because the entrance aperture was poorly collimated.

The measurement of the fractional increase in H_1^+ could not be completed. The methods are theoretically valid but technically hard to use. The measurement is important to show that the observed increases in the ion density are due to increased confinement.

VII. SUMMARY

This thesis has presented experimental results of electrostatic plugging of multidipole cusps. The results show increased ion and electron density and increasing plasma potential with increasing electrode bias. A model is presented and shown to give good qualitative agreement with the experiment. This work has also found and measured the contribution of secondary electrons to the plasma.

This work allows other experimentalists the ability to have "high" density plasmas at elevated plasma potentials. This freedom allows further investigation of secondary electrons, increasing the density of a particular ion species over another, or any other project requiring this combination of parameters.

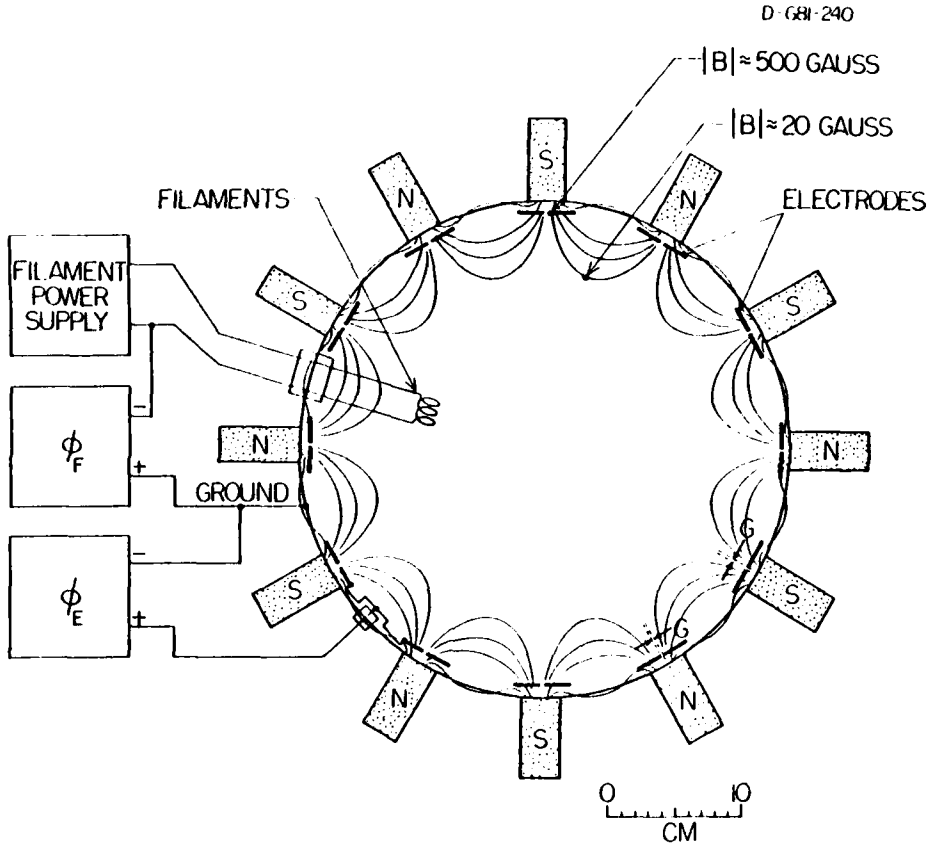

Figure 1. Electrode and magnetic field configuration in the e-pot devide. Filament and electrode biases voltages are shown schematically. Magnetic poles face the plasma and alternate in polarity as indicated. The magnet rows and electrodes are continued across the top and bottom.

A-682-187

LANGMUIR PROBE SWEEP CIRCUIT

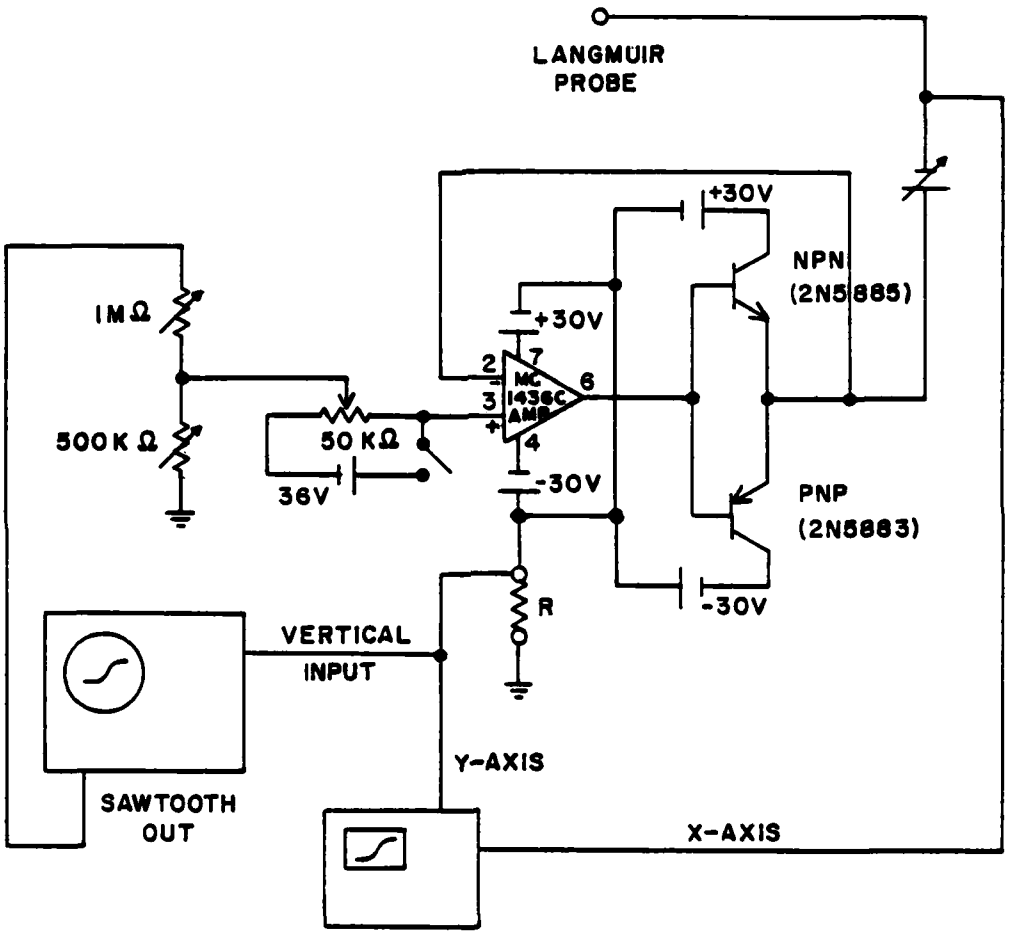

Figure 2. Schematic of Langmuir Probe sweep circuit.

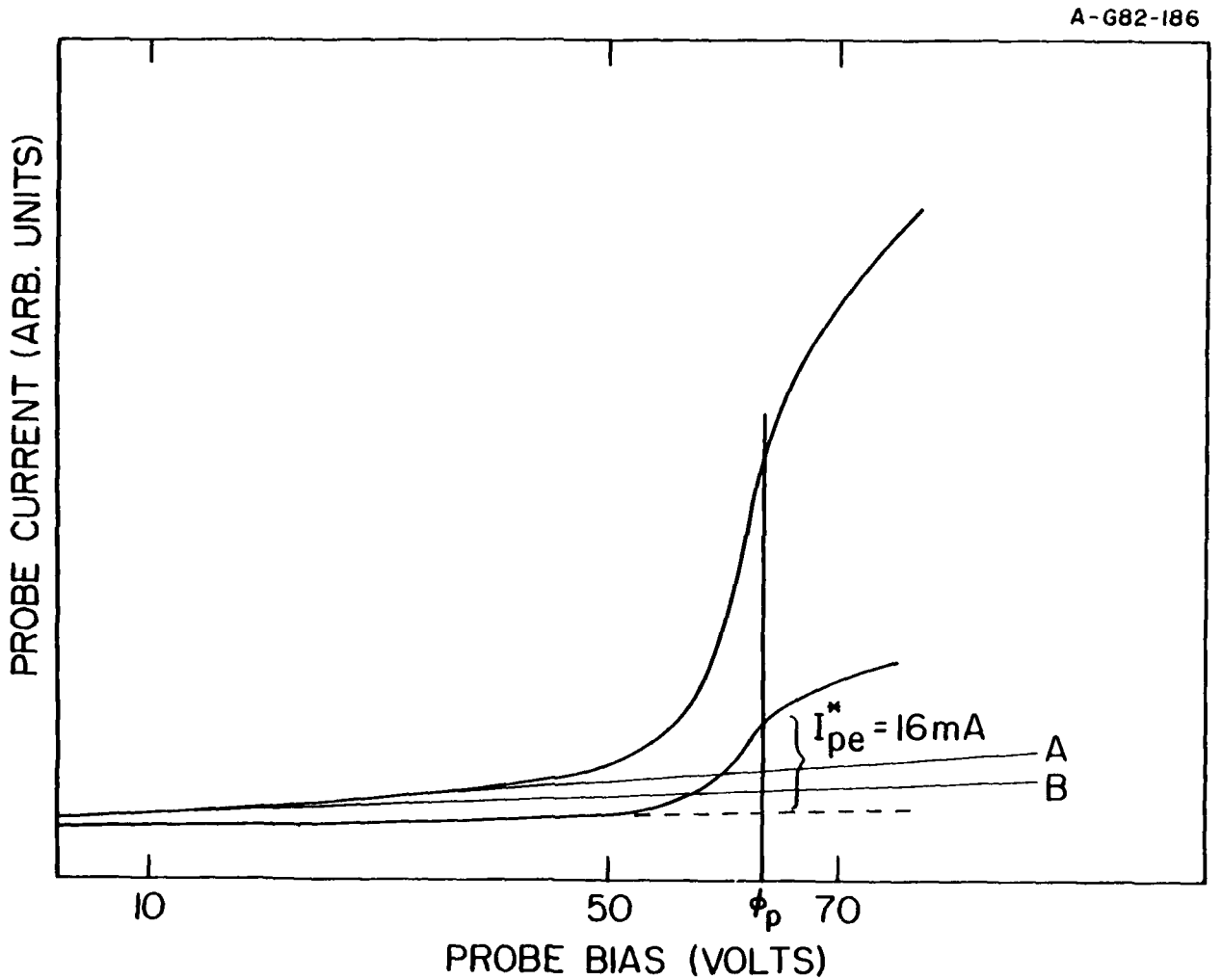

Figure 3. Typical Langmuir probe characteristic (without secondary electrons). The lines A and B subtract different amounts of primary electron current.

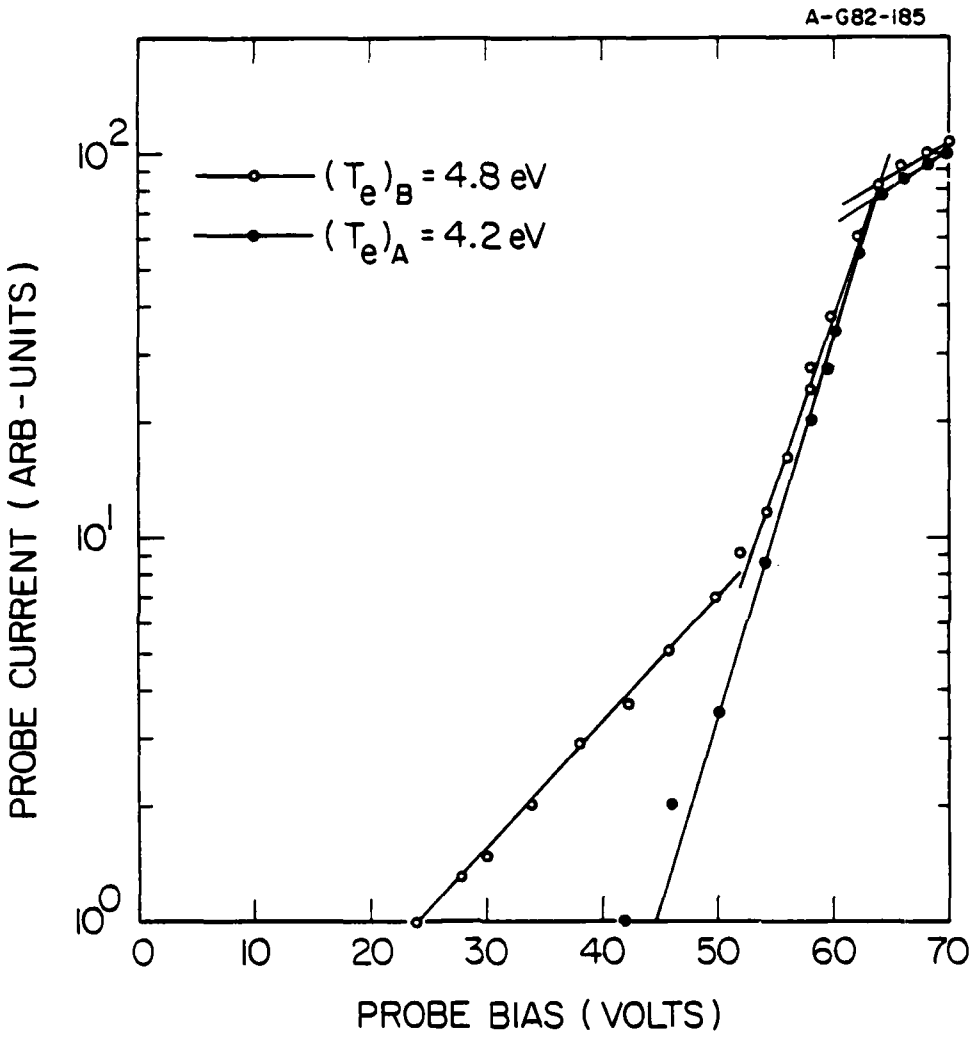

Figure 4. Semi-log plot of probe current vs. probe voltage (from Fig. 3). The effect of incorrectly removing the primary electrons is seen to raise the plasma electron temperature.

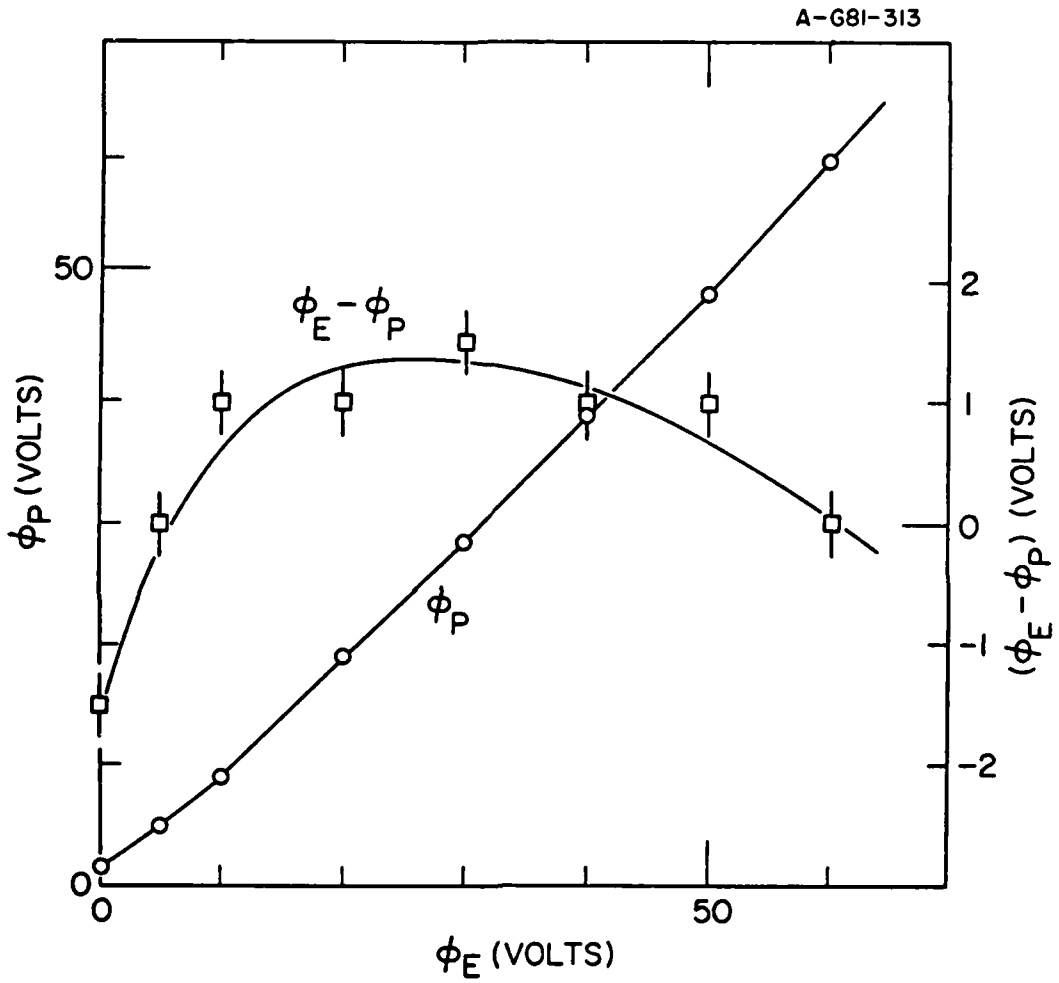

Figure 5. Plasma potential is the interior of the device versus electrode bias at 4×10^{-4} Torr with 12 mm electrode separation.

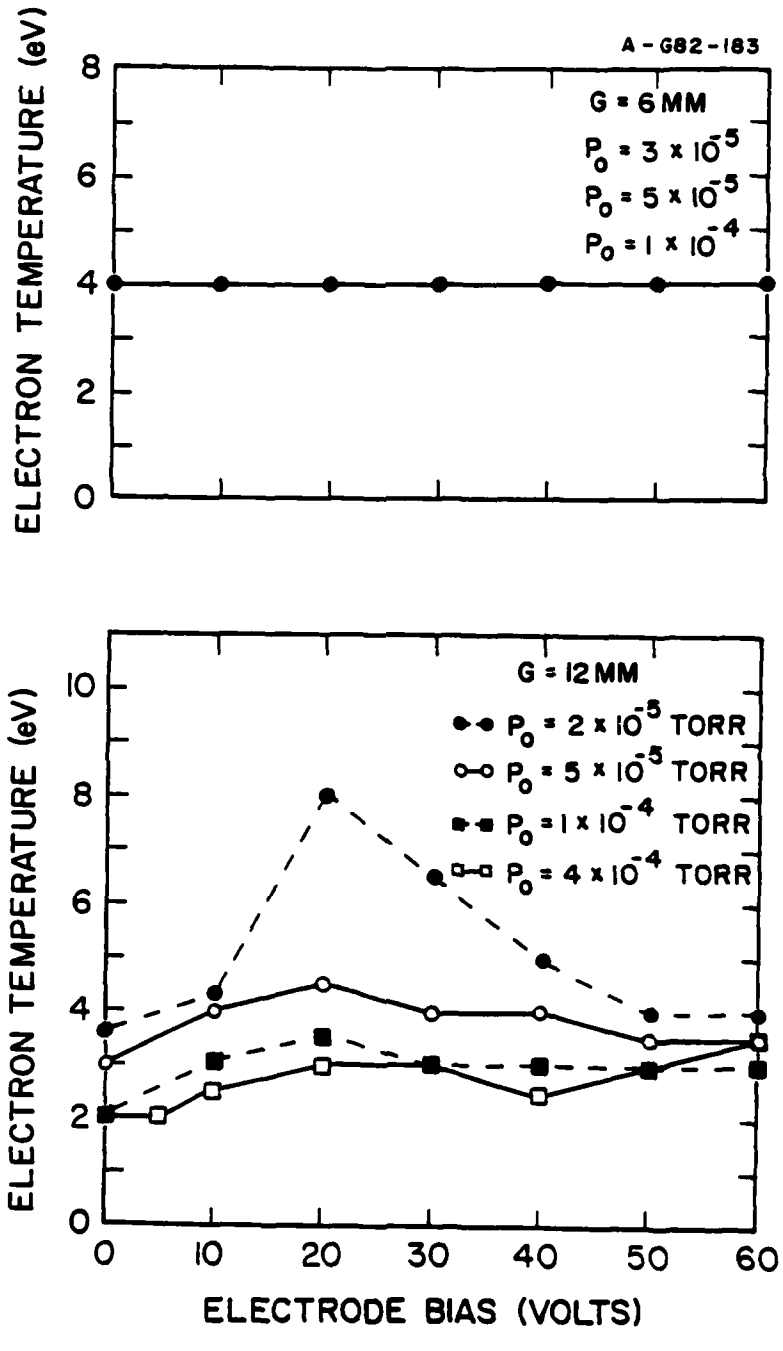

Figure 6. Variation of plasma electron temperature with electrode bias.

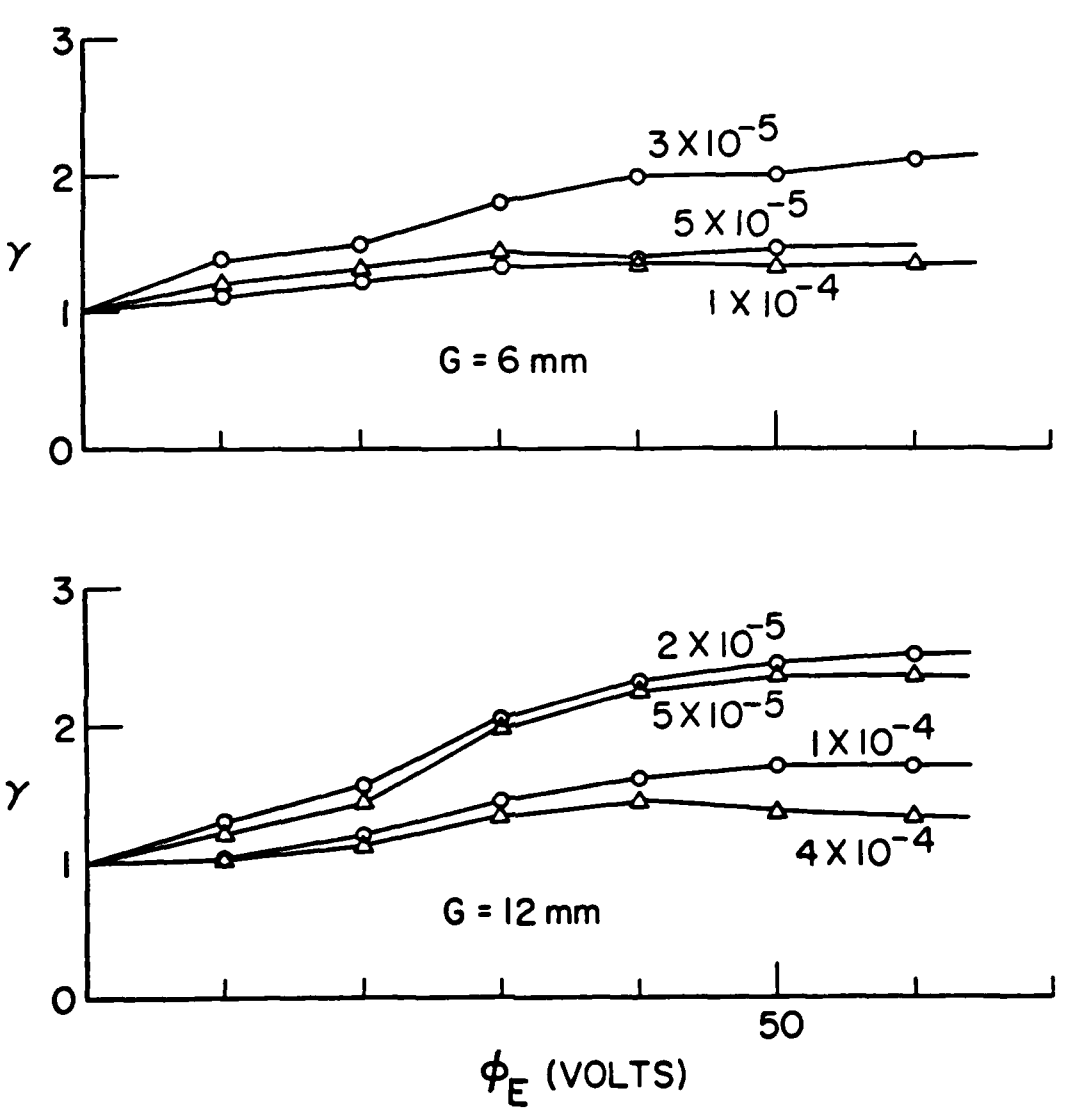

Figure 7. Plasma density versus electrode bias at several values of neutral pressure for 6 mm and 12 mm electrode separation (same data as Fig. 6).

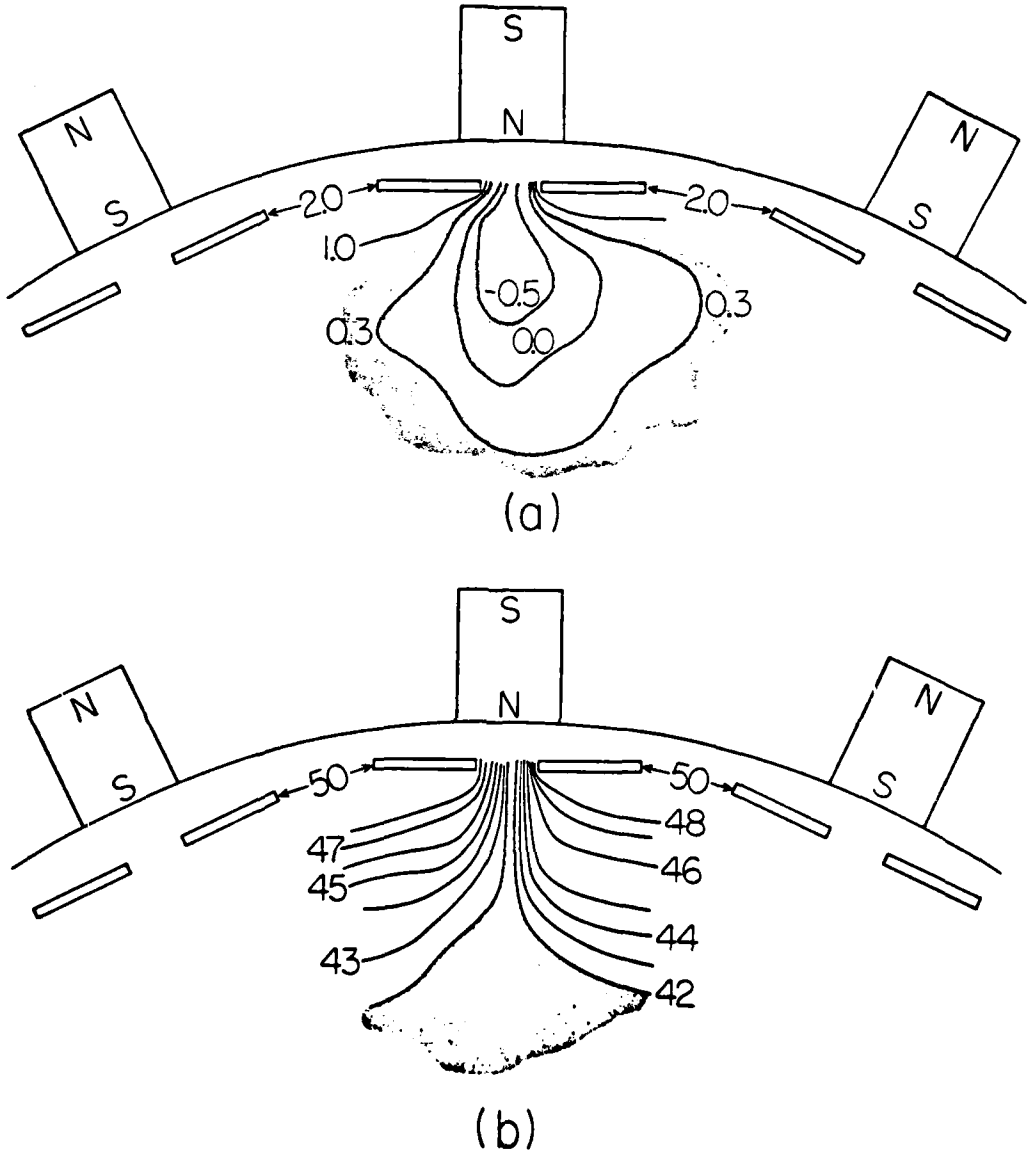

Figure 8. Equipotential contours (in volts) determined by an emissive probe.
a. Electrode bias at 2 V, neutral pressure equal to 8×10^{-5} Torr, $n = 2 \times 10^{9}$ cm^{-3}.
b. Electrode bias at 50 V, at 8×10^{-5} Torr, $n = 6 \times 10^{9}$ cm^{-3}.

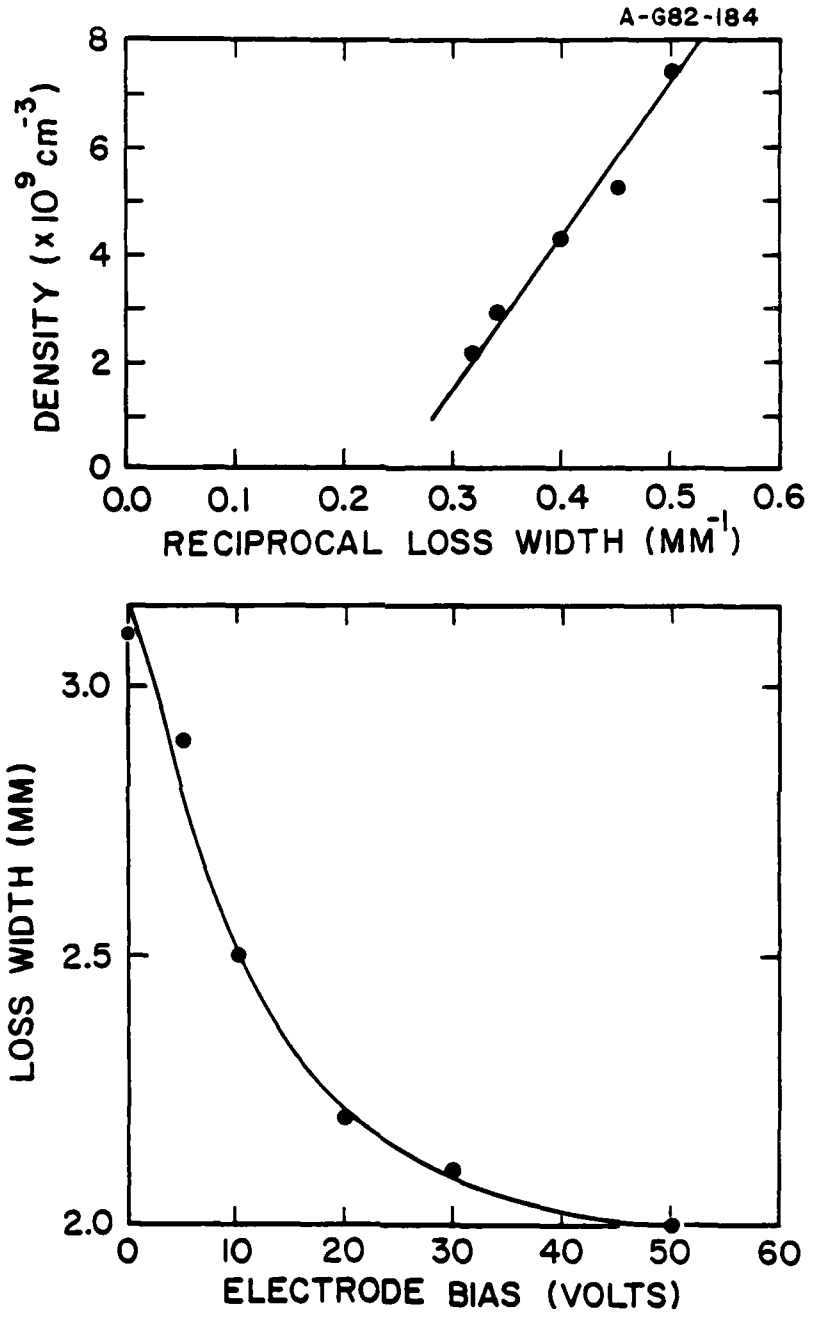

Figure 9. Variation of experimentally measured loss width with electrode bias. Upper figure shows linear relation between density and inverse loss width.

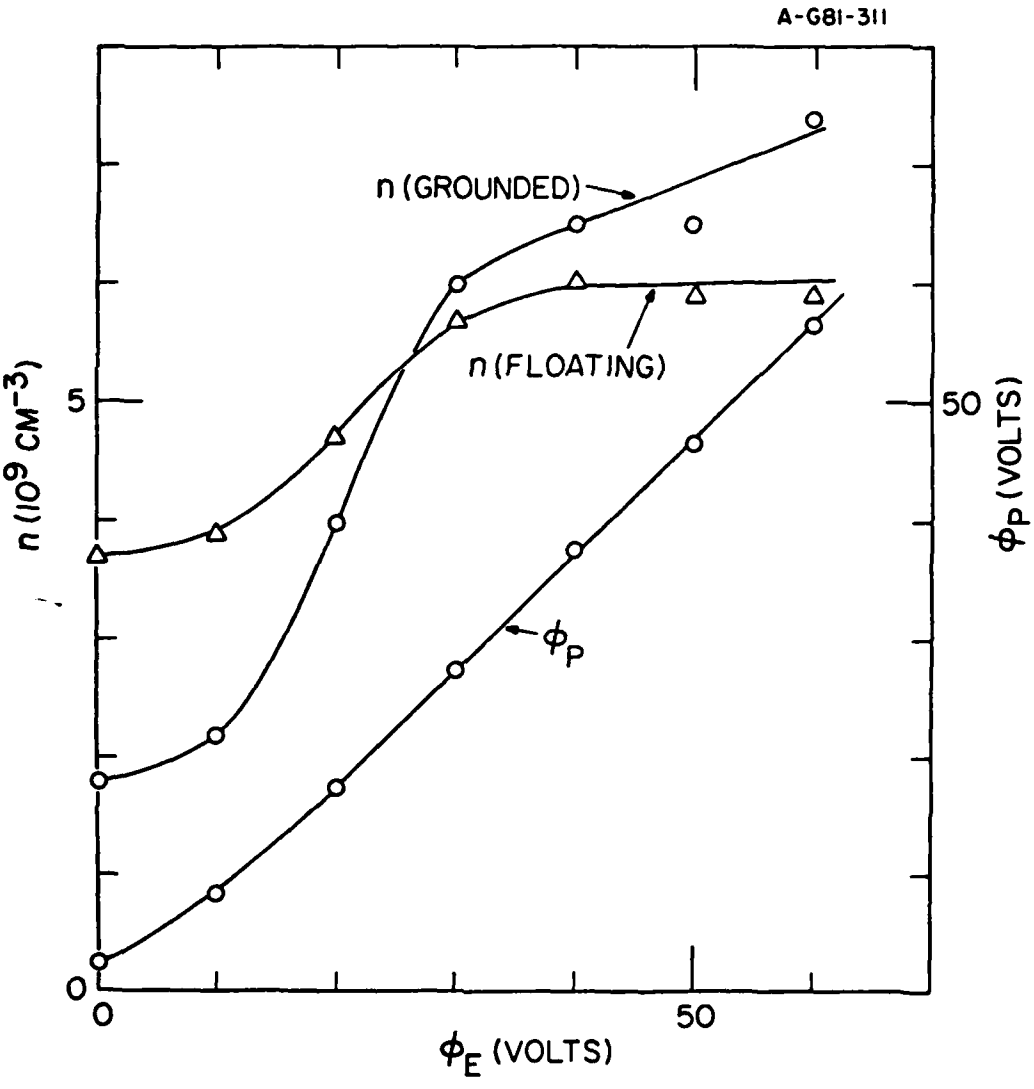

Figure 10. Plasma potential and density versus electrode bias Φ_E at 1×10^{-4} Torr in the presence of a large extraction grid. Data is given for floating and grounded grids.

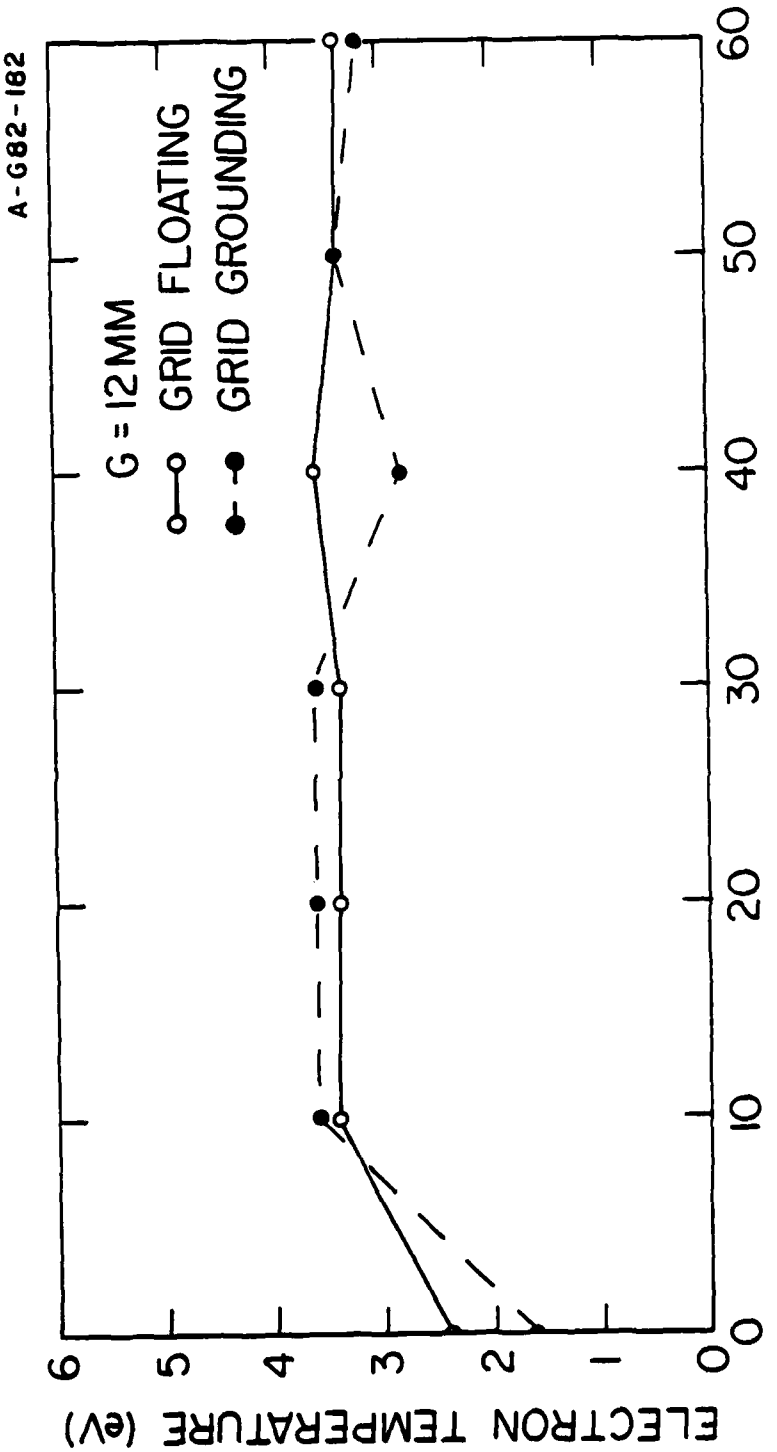

Figure 11. Variation of electron temperature with electrode bias in the presence of a grid (same data as Fig. 10).

B-G82-181

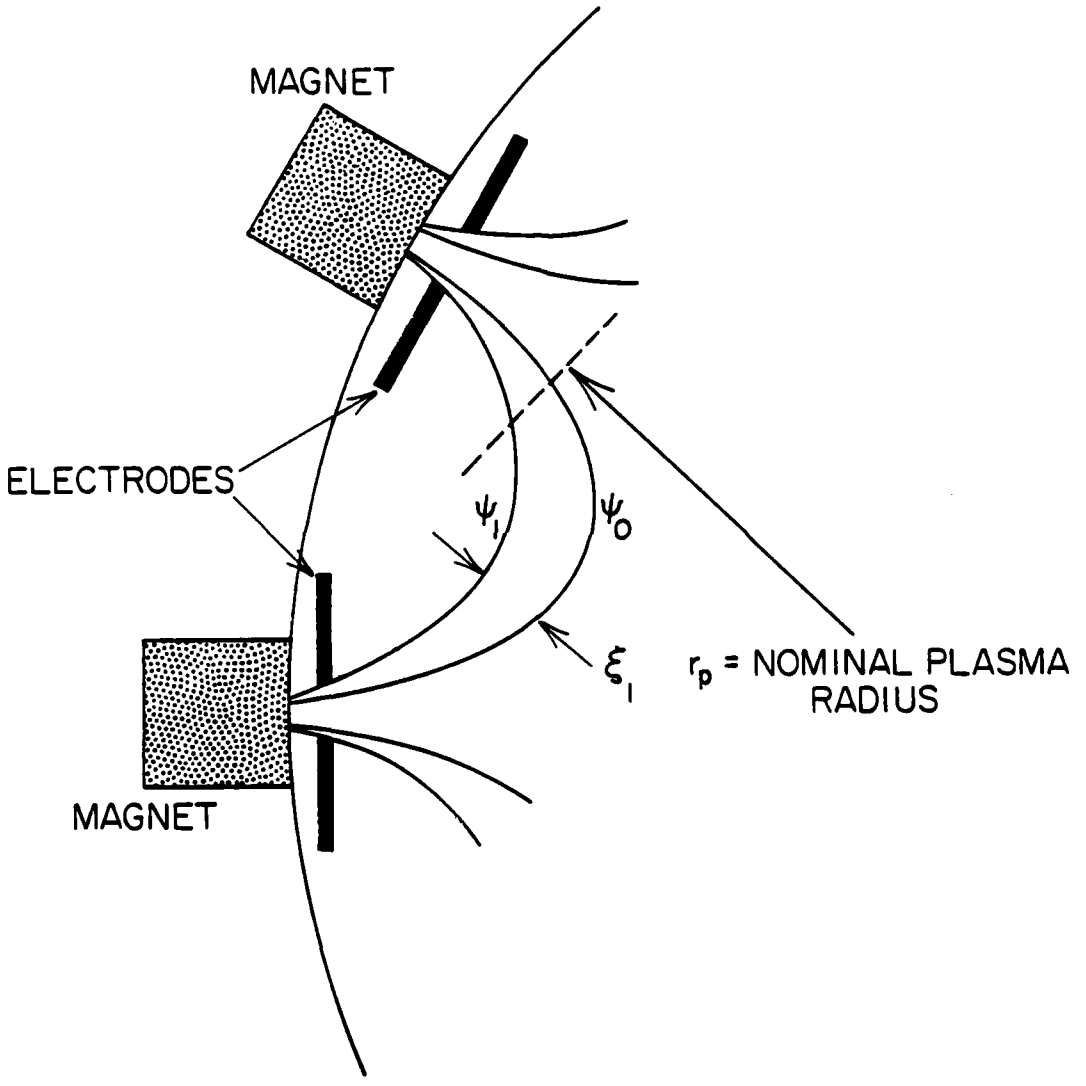

Figure 12. Geometry involved in Eq. (9).

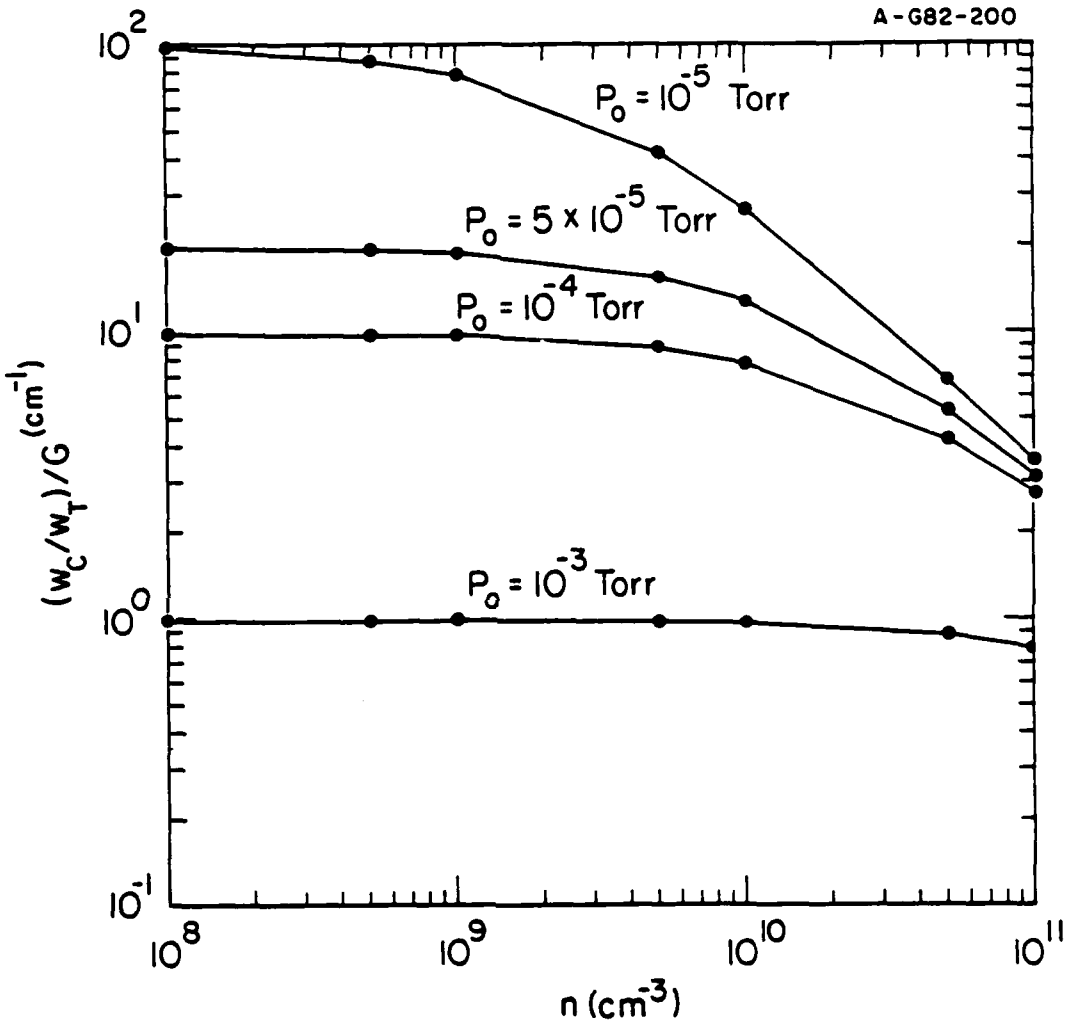

Figure 13. Graph of Eq. (26).

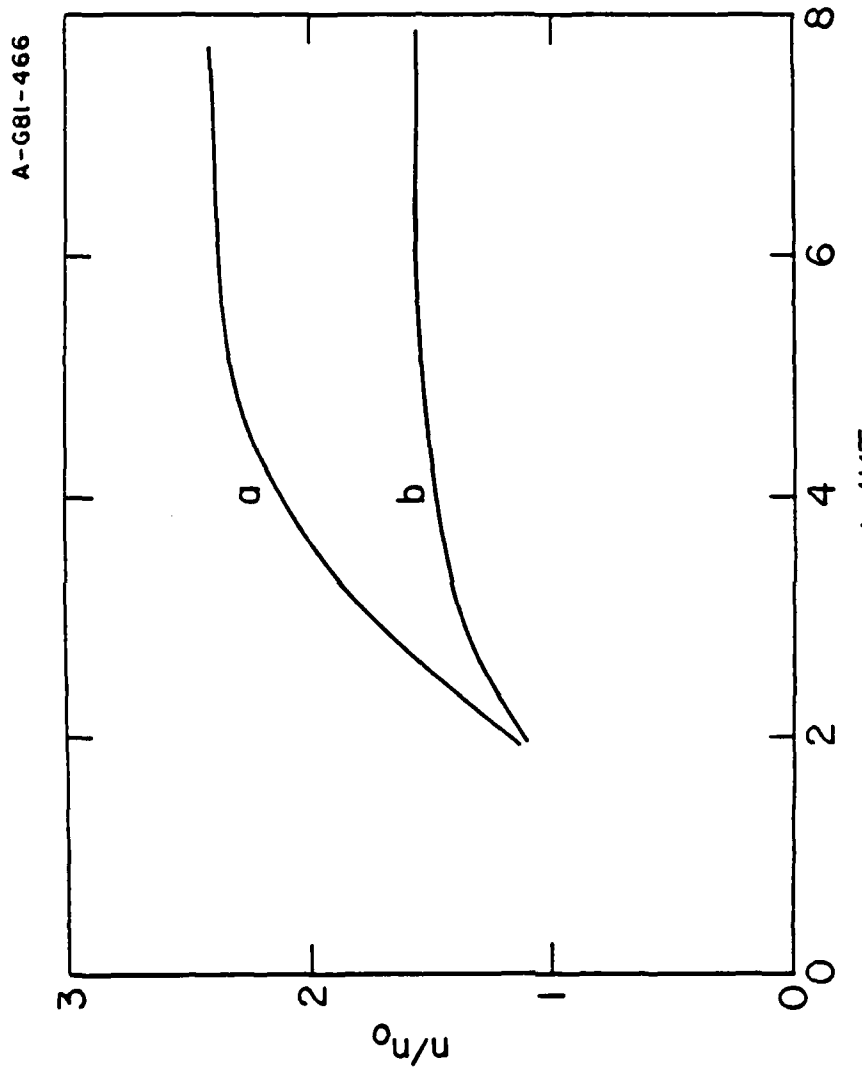

Figure 14. Model predictions of plasma density versus normalized electrode bias voltage e Φ_E/T_e.
a. Graph of Equation (46).
b. Graph of Equation (47).

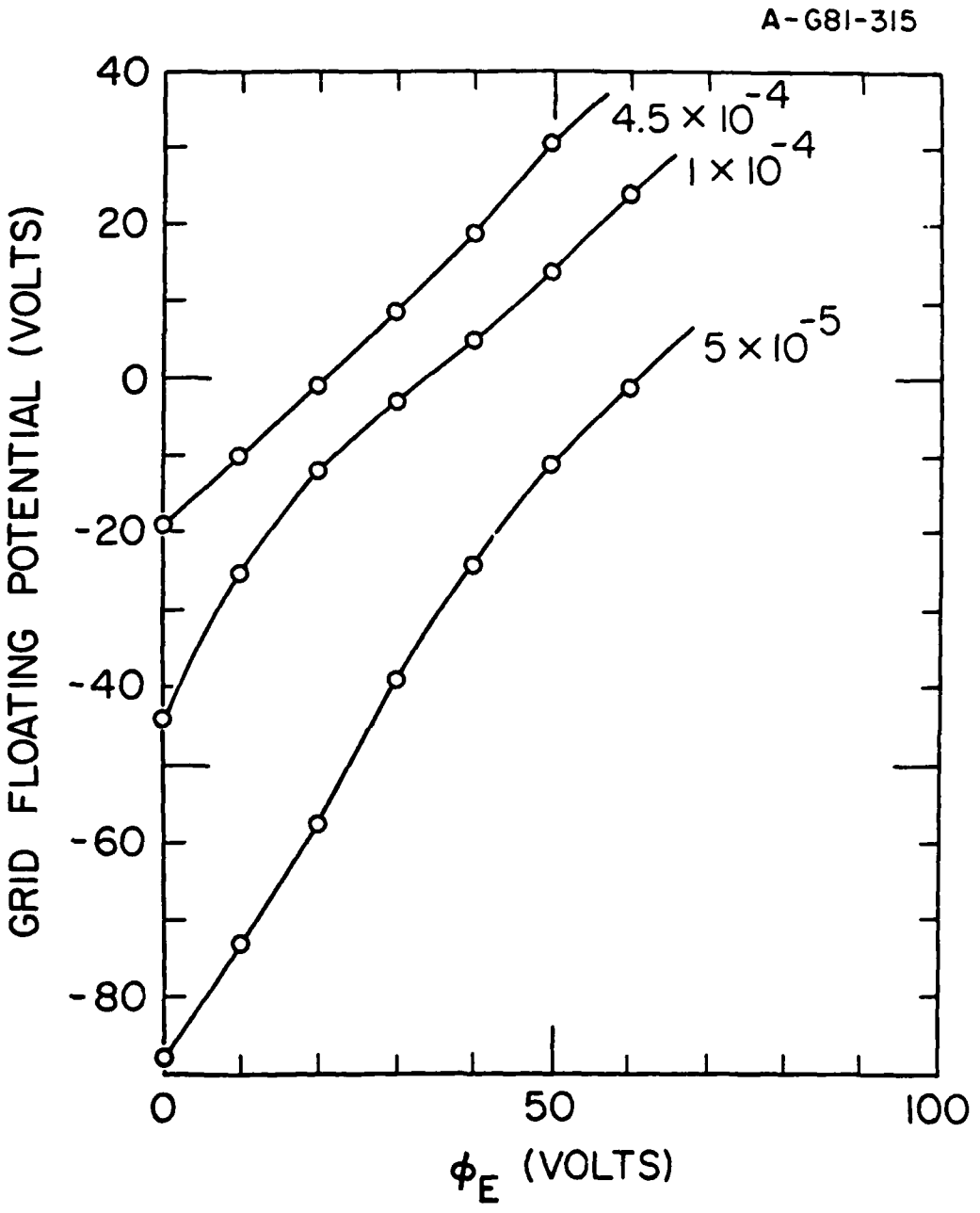

Figure 15. Grid floating potential versus electrode bias at several neutral pressures.

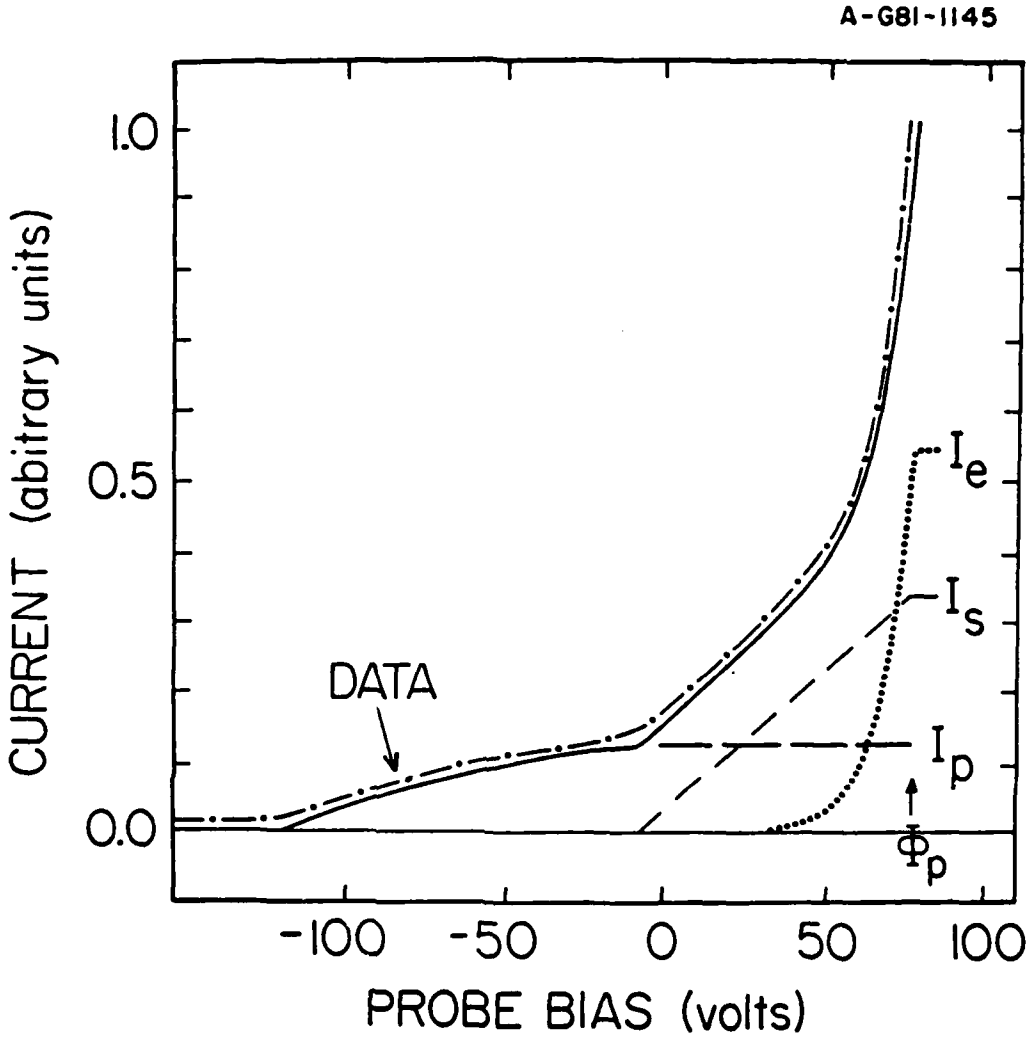

Figure 16. A representative Langmuir probe trace (labelled DATA). The plasma potential was 81.5 V. Data has been displaced slightly to allow comparison with the fit to the data. The contributions from the plasma electrons I_e, primary electrons I_p and secondary electrons I_s are separately indicated. The neutral pressure was 5×10^{-6} Torr.

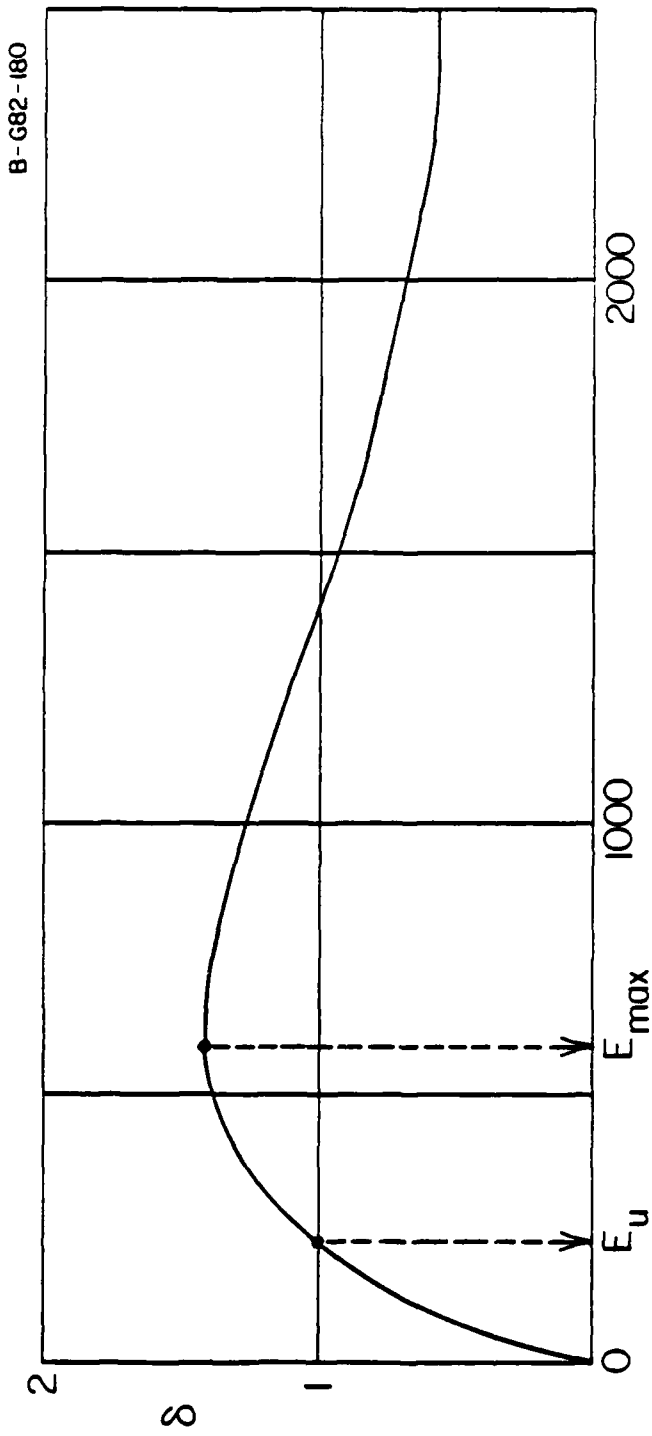

Figure 17. A typical graph of yield (δ) of secondary electrons from bombardment of chamber walls with primary electrons with energy E_p (from Hachenburg and Brauer).

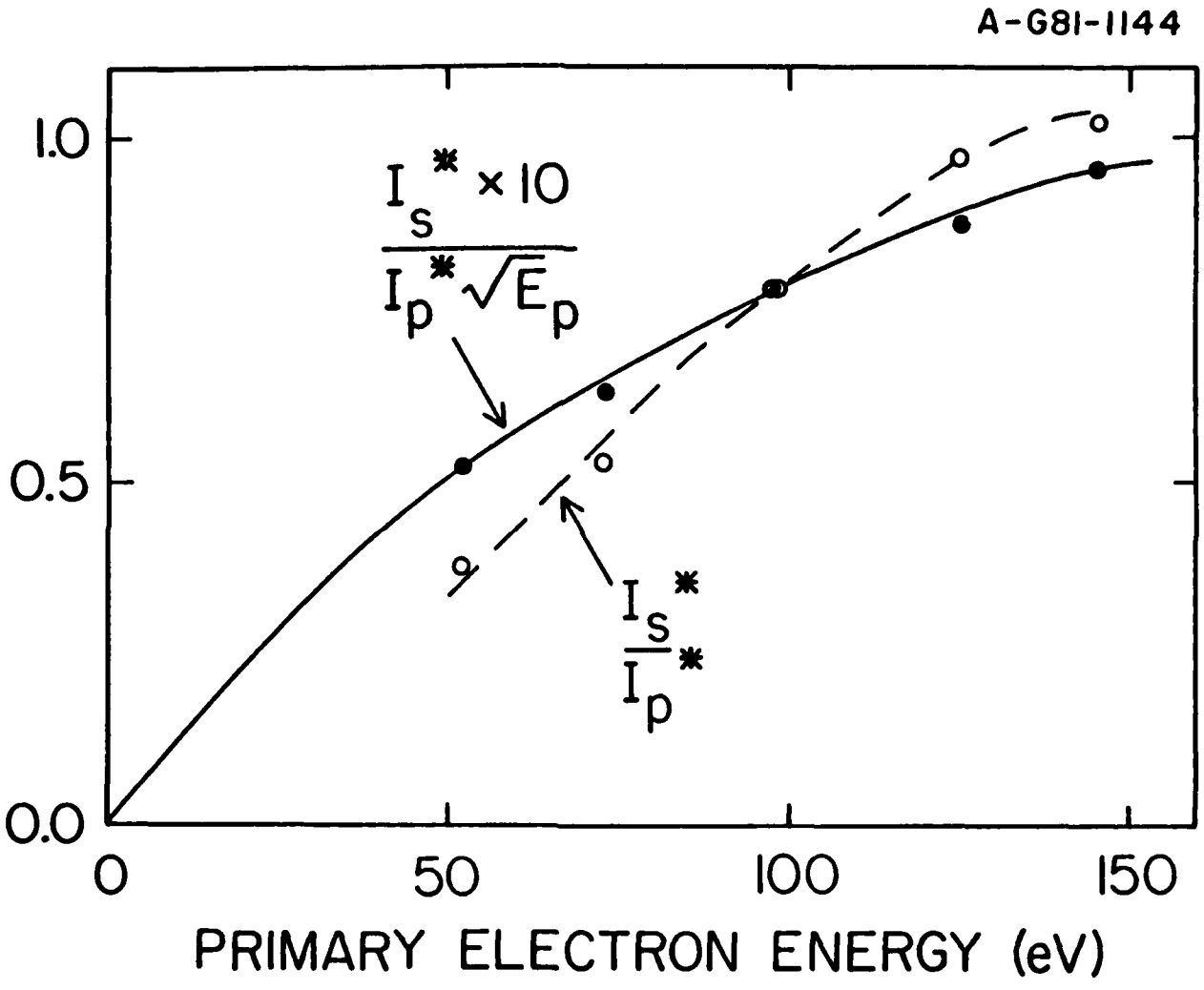

Figure 18. The ratios I_s^*/I_p^* and $10\ I_s^*/I_p^*\ \sqrt{E_p(eV)}$ versus primary electron energy.

A-682-179

MASS SPECTROMETER CIRCUIT

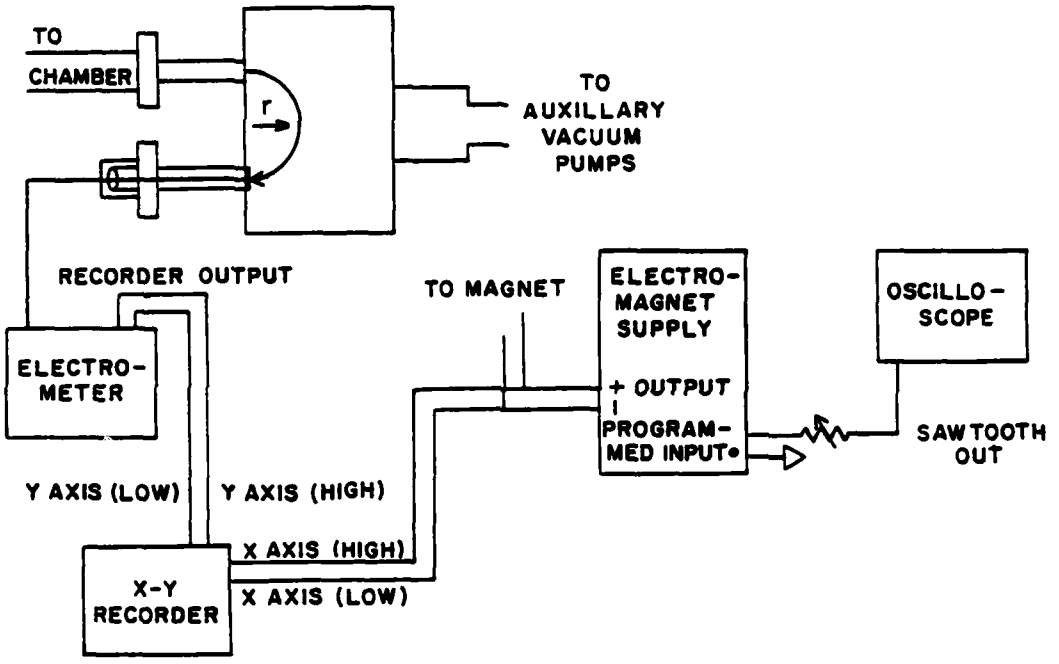

Figure 19. Schematic of externally mounted mass spectrometer experiment.

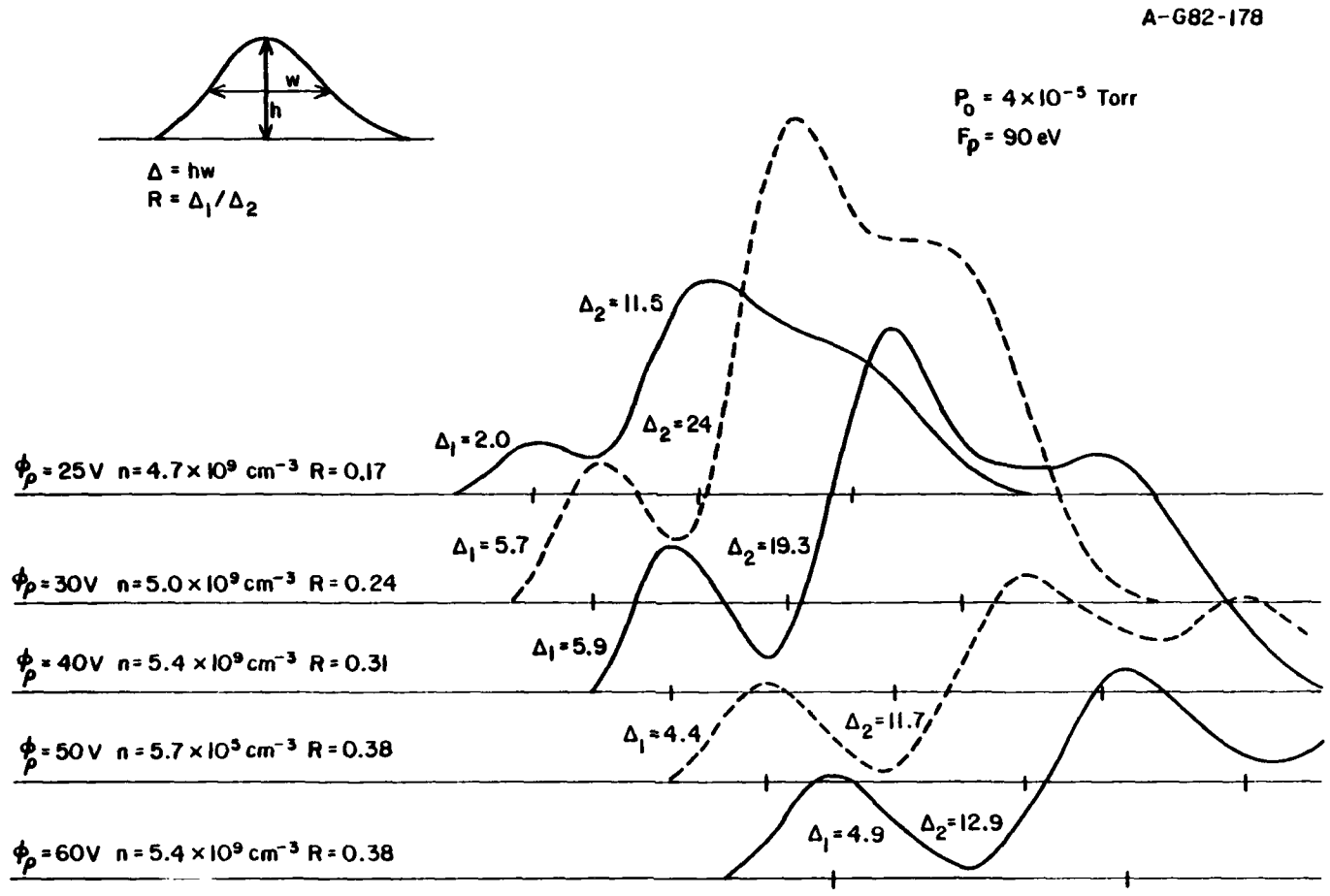

Figure 20. Representative spectrograph of a hydrogen plasma.

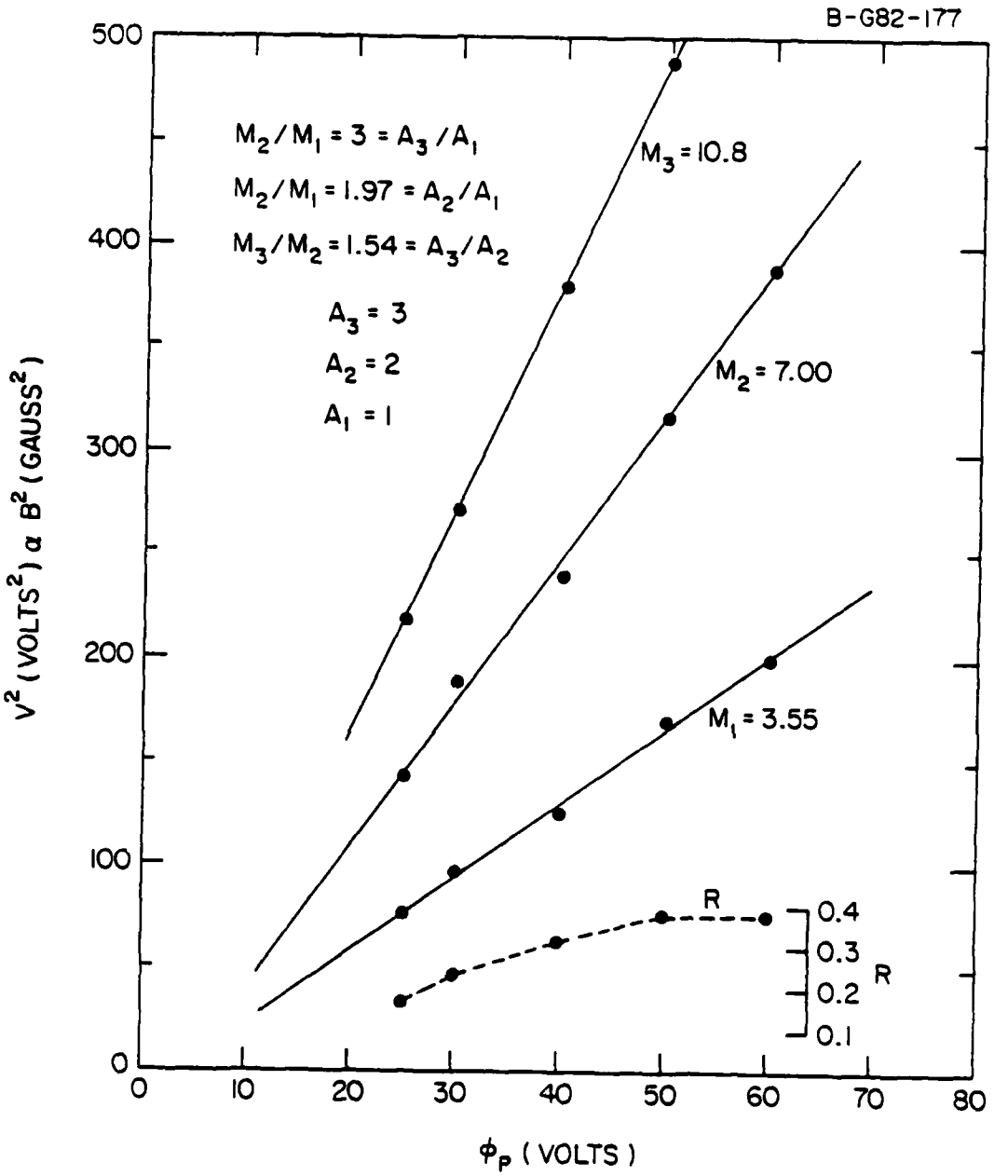

Figure 21. Top three curves show the square of magnetic field for maximum flux vs. plasma potential. The bottom graph shows variation of density of atomic hydrogen to molecular hydrogen with plasma potential when E_p = 90 V and $p_o \sim 4 \times 10^{-5}$ Torr.

REFERENCES

[1]R. Limpaecher and K. R. Mackenzie, Rev. Sci. Instrum. 44, 726 (1973).

[2]R. L. Hirsch, J. Appl. Phys. 38, 4522 (1967).

[3]N. Hershkowitz, K. N. Leung, and T. Romesser, Phys. Rev. Lett. 35, 277 (1975).

[4]A. Kitsunezaki, M. Tanimoto, and T. Sekiguchi, Phys. Fluids 17, 1895 (1974).

[5]T. J. Dolan, B. L. Stansfield, and J. M. Larsen, Phys. Fluids 18, 1383 (1975).

[6]T. J. Dolan, J. M. Larsen, and B. L. Stansfield, Can. J. Phys. 53, 2341 (1975).

[7]Noah Hershkowitz, Kyle Hendricks, and R. T. Carpenter, submitted to J. Appl. Phys.

[8]K. N. Leung, N. Hershkowitz, and K. R. Mackenzie, Phys. Fluids 19, 1045 (1976).

[9]Noah Hershkowitz, R. L. Goettsch, Chung Chan, Kyle Hendricks, and R. T. Carpenter, submitted to J. Appl. Phys.

[10]D. Rapp and P. Englander-Golden, J. Chem. Phys. 43, 1464 (1965).

[11]A. Lang and N. Hershkowitz, J. Appl. Phys. 49, 4707 (1978).

[12]J. R. Smith, N. Hershkowitz, and P. Coakley, Rev. Sci. Instrum. 50, 210 (1979).

[13]T. J. Dolan, Lawrence Livermore Laboratory, Report UCRL-52142.

[14]S. R. Seshadri, Fundamentals of Plasma Physics, American Elsevier Publishing Co., 415 (1973).

[15]H. B. Milloy, R. W. Crompton, J. A. Rees, and A. G. Robertson, Aust. J. Phys. 30, 61 (1977).

[16]T. Samec and R. Stenzel, Bull. Am. Phys. Soc. 17, 1017 (1972).

[17]T. Samec, K. N. Leung, K. R. Mackenzie, and B. D. Fried, Bull. Am. Phys. Soc. 19, 928 (1974).

[18]G. Knorr and C. K. Goertz, Astrophys. and Space Sci. 31, 209 (1974).

[19]G. Hachenburg, W. Brauer, Advances in Electronics and Electron Physics XI, (L. Marton, Ed.), Academic Press, New York, 413 (1959).

[20]K. W. Ehlers and K. N. Leung, Rev. Sci. Instrum. 50, 1353 (1979).

[21]I. Alexeff, W. D. Jones, and K. Lonngren, Phys. Rev. Lett. 21, 878 (1968).

[22]K. W. Ehlers, K. N. Leung, and M. D. Williams, Lawrence Livermore Laboratory, Report LBL-8863.